Coordination Chemistry Reviews 449 (2021) 214183

Contents lists available at ScienceDirect

Coordination Chemistry Reviews

journal homepage: www.elsevier.com/locate/ccr

Review

# Porphyrin silanes

Julia E. Pia [a], Burhan A. Hussein [a,b], Vladislav Skrypai [c], Olga Sarycheva [a], Marc J. Adler [a,*]

[a] Department of Chemistry & Biology, Ryerson University, 350 Victoria St., Toronto, ON M5B 2K3, Canada
[b] Department of Chemistry, Durham University, Durham DH1 3LE, United Kingdom
[c] Department of Chemistry & Biochemistry, Northern Illinois University, DeKalb, IL 60115, USA

ARTICLE INFO

*Article history:*
Received 16 March 2021
Accepted 22 August 2021

*Keywords:*
Porphyrins
Silanes
Silicon

ABSTRACT

Porphyrin silanes (PorSils) are a unique class of metalloporphyrins that contain a hexacoordinate silicon center. This review chronicles the comprehensive body of research on PorSils to-date, beginning with their first discovery in 1967 by Boylan and Calvin. In the intervening five-plus decades, the synthesis of PorSils have been varied and optimized. PorSils possessing a variety of substituents – both axial and peripherally – have been reported; such functionalization can impact the properties with electronic and/or steric influence. We explore the structural, physical, electronic, and spectral attributes of PorSils, outlining and comparing this data. The unique properties of PorSils have widened the scope for the applications of metalloporphyrins: researchers have reported the use of PorSils for GC/MS analysis, electric and photoelectric applications, dual luminophores for pressure and oxygen sensing, photocatalysis, and photodynamic therapy. This review provides the first comprehensive summary of the development of PorSils, their unique features, and their contribution to the field of porphyrin chemistry.


**Contents**



* Corresponding author.
*E-mail address:* marcjadler@ryerson.ca (M.J. Adler).

https://doi.org/10.1016/j.ccr.2021.214183
0010-8545/

## 1. Background and importance

The word "porphyrin" is derived from the Greek word "porphua", meaning "purple" [1]. The class of molecules we call porphyrins are indeed typically purple, and are aromatic macrocyclic rings comprised of four pyrrole rings connected by methine bridges (Fig. 1a) [1–3]. Porphyrins are naturally occurring and many synthetic variants [4–9] have been made; they have found application in a wide range of fields such as alternative energy [10], medicine [11–13], and supramolecular chemistry [14,15].

Structurally, porphyrin rings have several functionalization sites that can modify the compound's character: a *meso* position, $\beta$ position, inner nitrogen atoms, and (if *N*-metallated to make metalloporphyrins) a metal center. (Fig. 1b) [16]. Such substitution can improve the porphyrin's solubility – an inherent issue with these large, flat, aromatic macrocycles – and can alter the optical and electronic properties of the compound [2,16].

Well-known metalloporphyrins include iron porphyrins, such as heme, and magnesium porphyrins, such as chlorophyll (which actually contains a reduced porphyrin known as a chlorin) [1]. While many metalloporphyrins are well-established, the growth of main group porphyrin chemistry has fallen behind that of their transition metal analogs; this is likely due to their perceived biological irrelevance and challenging syntheses [17]. Of these neglected main-group analogs, silicon (IV) porphyrins (PorSils) are particularly intriguing derivatives since silicon is the second most abundant element on Earth, which makes it highly amenable to large-scale materials applications (e.g. as in polymers [18] and photovoltaics) [19,20].

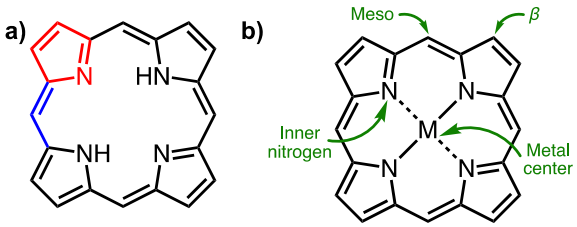


**Fig. 1. Porphyrin Structure. a)** Porphyrin's macrocyclic structure consisting of pyrrole rings (red) connected by methine bridges (blue), **b)** functional sites of porphyrin complexes (green).

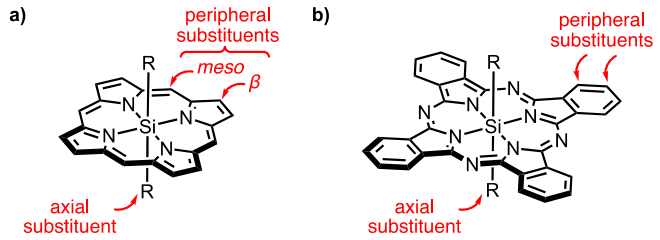


**Fig. 2. General Structure of a) PorSil and b) PcSil.** The silicon center introduces axial substituents (R), in addition to the peripheral substituents that can be installed.

First reported in 1967 by Boylan and Calvin, PorSils offered a new class of hexacoordinate silicon compounds [21]. The central silicon allows for an additional functionalization site within the porphyrin complex; silicon's 3-center 4-electron bond allows for hypercoordination and the introduction of covalently attached axial ligands [22]. Symmetric (Por)$SiX_2$ compounds were explored first; however, several PorSil complexes were made with different *trans* ligands to better understand this hypercoordinate bond [23]. The properties of PorSils can be further modified by varying the groups in the axial position (Fig. 2a), which widens the properties and application scope of porphyrins.

In contrast to PorSils, there are many reports of phthalocyanines (Pcs) – synthetic porphyrins analogs containing four nitrogen-bridged isoindole units (Fig. 2b) – containing a central silicon atom [24]. Both macrocycles can be metallated, substituted, and form hexacoordinate complexes [25,26]. A wide variety of silicon Pcs (SiPcs) have been explored and reported; axial ligands have enhanced photosensitivity, improved solubility, and reduced aggregation within Pcs [26–30]. Though there are numerous SiPcs reported, they often suffer from poor solubility [25,28–31]. Lemke et al. identified that PorSils are a more attractive candidate for hexacoordinate silicon complexes due to an improved solubility and a wide range of accessible peripherally substituted derivatives [25,31].

The properties and applications of Pcs and porphyrins are both distinct and complimentary to one another. Pcs are known for their thermal and chemical properties, as well as their optoelectronic and magnetic properties [24]. Their absorption spectrum varies from that of porphyrins, as they commonly absorb in the near infrared region [24]. Their properties have enabled them to be successful in many applications, such as organic light emitting diodes (OLEDs), redox-dependent fluorophores, and dye sensitized solar cells (DSSCs) [24].

Porphyrins are known for their chemical and chromophoric properties, biological functions, and redox activity. Porphyrin compounds have high absorptivity in the visible and NIR spectral regions, which can be used to harvest light for photovoltaic applications [32]. Photochemical and spectroscopic properties of porphyrins are interesting not only because of their importance in natural photosynthesis but also for their utility as novel materials. Porphyrins are applied as intermediates in key biological processes, such as artificial photosynthesis and catalysis [33,34]. They

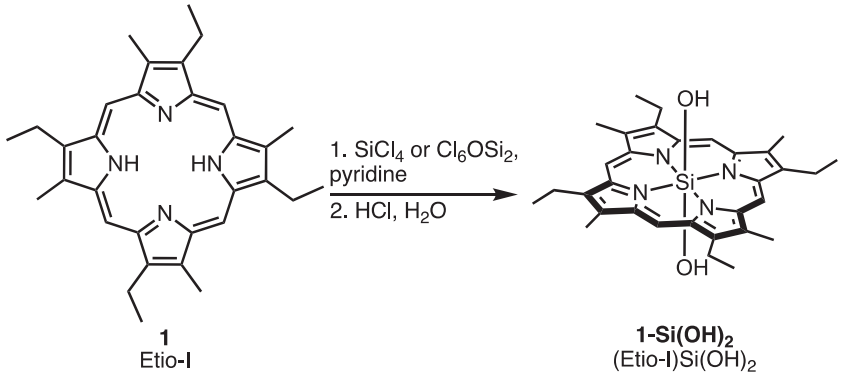


**Fig. 3. First Synthesis of (Etio-I)Si(OH)$_2$.** First reported synthesis of a PorSil, known as (Etio-I)Si(OH)$_2$ (**1-Si(OH)$_2$**), by Boylan and Calvin.

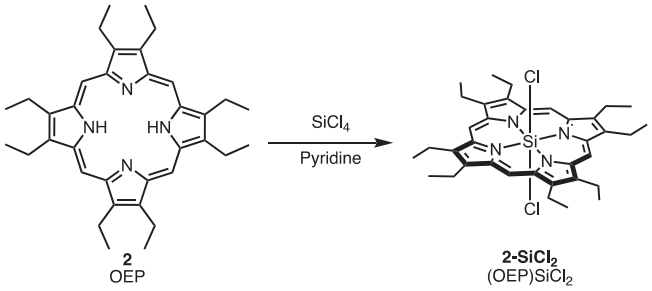


**Fig. 4. First Synthesis of (OEP)SiCl$_2$.** First reported synthesis of (Por)SiCl$_2$, by Gouterman et al. **2** was reacted with pyridine and silicon tetrachloride to produce (OEP)SiCl$_2$ (**2-SiCl$_2$**).

also partake in applications as isostructural dopants for organic semiconductors [35].

Reviews have been conducted for specific metalloporphyrins, as well as metalloporphyrin applications in general [36,37]. There have not been any comprehensive outlooks reported specifically on PorSils. The field of PorSils holds great promise due to the unique attributes of the central silicon, including its inertness, abundance in nature, and its ability to offer additional covalent functionalization sites of porphyrins through the introduction of axial ligands. This modification expands the scope of metalloporphyrins, making it an attractive feature for various biological and functional materials applications.

Herein, a comprehensive literature review of PorSils is provided, in which the development of their synthesis is chronicled, their structural and electronic properties are described, and the known applications of PorSils are outlined. This review aims to highlight the importance of PorSils and will serve as a foundation for future work involving PorSils.

A brief note on nomenclature: the formal IUPAC name for the core structure of the title compounds – using the accepted trivial name "porphyrin" for the tetrapyrrolic core – would be "-porphyrinatosilicon" [38]. In practice, researchers have favoured the use of either "porphyrin silanes" or "silicon porphyrins", and in our opinion either of these are generally acceptable ways to refer to this class of molecules. People who come into this field from an inorganic/organometallic/porphyrin chemistry background may be most comfortable with the phrase "silicon porphyrin" as this approach is in line with how metalloporphyrins and related compounds are practically described, e.g. "iron porphyrin" or "silicon phthalocyanine". In our research group, we prefer "porphyrin silanes" given our perspective as organosilicon/organic chemists. "Silane" strictly implies compounds that only contain Si-H or Si-Si bonds, but the phrase is also commonly used to describe a variety of compounds containing molecular silicon: e.g. molecules containing Si-C bonds, which are also more specifically called "organosilanes" [39]. Analogously, molecular silicon (i.e. a "silane") that is bonded to a porphyrin can reasonably be referred to as a "porphyrin silane". For the sake of clarity, we refer to these compounds only as "porphyrin silanes", or "PorSils" for short, throughout this review. However, we make no claim that this name is any more or less appropriate than any another that can aptly communicate the essence of the structure.

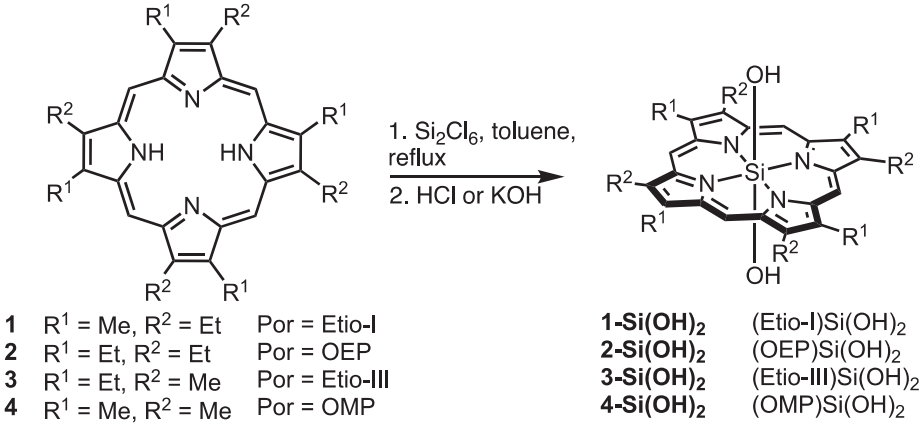


**Fig. 5. Simplified Synthesis of (Por)Si(OH)$_2$ via Reflux.** In addition to **1-Si(OH)$_2$**, Marriot et al. synthesized **2-Si(OH)$_2$** to **4-Si(OH)$_2$** by refluxing the base porphyrin in the presence of toluene and hexachlorodisilane, followed by hydrolysis.

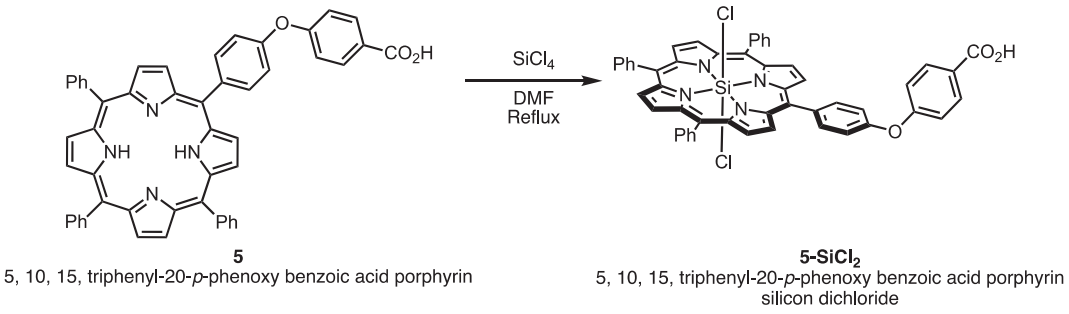


**Fig. 6. Reflux Method to Produce 5-$SiCl_2$.** Managa et al. exposed **5** to DMF and silicon tetrachloride under reflux to produce **5-$SiCl_2$**.

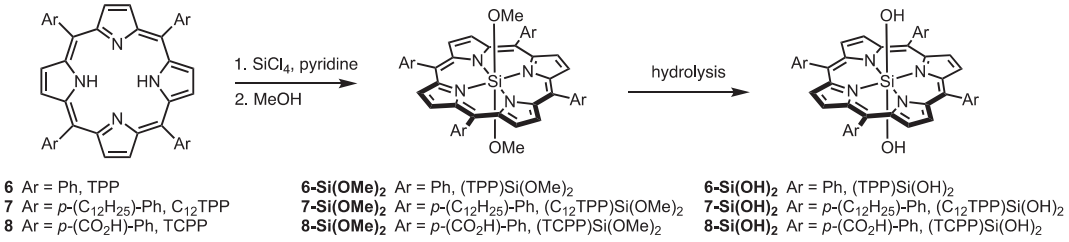


**Fig. 7. Formation of (Por)$Si(OH)_2$ from an Intermediate.** Base porphyrin was converted to the intermediate, (Por)$Si(OMe)_2$, which was hydrolyzed using a base or solvent.

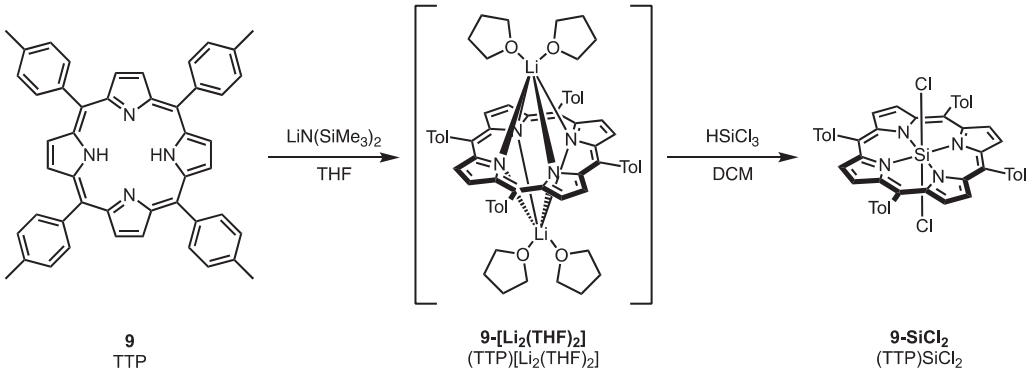


**Fig. 8. Synthesis of 9-$SiCl_2$ from a Lithium Salt Intermediate.** TTP (**9**) was converted to a lithium salt intermediate, which was easily silylated by a hydrochlorosilane. This evaded the stability issues observed when trying to silylate **9** using Gouterman's method. [25]

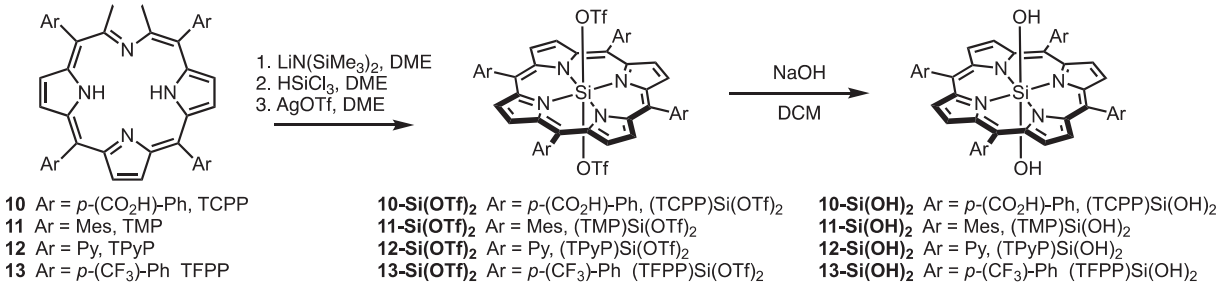


**Fig. 9. Formation of (Por)$Si(OH)_2$ from a (Por)$Si(OTf)_2$ Intermediate.** A three-step one pot synthesis was conducted to produce the (Por)$Si(OTf)_2$ intermediate, which was hydrolyzed to produce the (Por)$Si(OH)_2$ building block[31,54,20].

## 2. Synthesis

### 2.1. (Por)$SiCl_2$ and (Por)$Si(OH)_2$ building blocks

#### 2.1.1. Use of silicon tetrachloride, hexachlorodisiloxane, or hexachlorodisilane

(Por)$SiCl_2$ and (Por)$Si(OH)_2$ are often used as basic building blocks for the synthesis of PorSil derivatives. The first synthesis of a PorSil was reported in 1967 by Boylan and Calvin, in which etioporphyrin I (Etio-I) (1) was reacted with silicon tetrachloride or hexachlorodisiloxane and anhydrous pyridine [21]. This was followed by hydrolysis in dilute aqueous ethanolic hydrochloric acid (Fig. 3) to give (Etio-I)$Si(OH)_2$ (**1-Si(OH)$_2$**) [21,40]. The conversion of the base porphyrin to the PorSil complex is observed by a fluorescence colour change from deep red to orange under a 360 mμ lamp [40].

In 1973, Gouterman et al. reported the first isolation of (Por)$SiCl_2$ by reacting octaethylporphyrin (OEP) (**2**) with pyridine and silicon tetrachloride (Fig. 4) [41,42]. In 1978, Buchler identified that the hydrolysis of this compound can occur during chromatography [43]. Buchler also noted that the synthesis of metalloporphyrins often involves the use of glacial acetic acid; however, some tetravalent metals are labile towards acid and this method cannot be used to install the silicon center in porphyrin complexes [43]. Pyridine is an effective solvent due to its basic properties [43], however silicon-pyridine complexes can form, which can slow the reaction and lead to longer reaction times or incomplete reactions [43].

In 1982, Marriot et al. simplified Boylan and Calvin's procedure and introduced a reflux method in order to synthesize several different compounds of the general structure (Por)$Si(OH)_2$ (Fig. 5) [44]. Dry toluene solvent and an inert atmosphere was required to prevent moisture from consuming the hexachlorodisilane, which, when reacted with the porphyrin of interest, yielded (Por)$SiCl_2$ [44]. They conducted the hydrolysis of (Por)$SiCl_2$ with hydrochloric acid, but identified that this step may be a drawback because some porphyrin could be irreversibly trapped in the solid silicon dioxide by-product matrix [44]. In 1984, Marriot et al. further modified their hydrolysis step with the use of aqueous KOH [45–47].

Managa et al. also applied this reflux method by reacting 5, 10, 15, triphenyl-20-*p*-phenoxy benzoic acid porphyrin (**5**) with silicon tetrachloride and DMF in order to install the silicon dichloride center, seen as **5-SiCl$_2$** in Fig. 6 [48].

In 1988, Buchler et al. followed a different path for the production of (Por)$Si(OH)_2$, using tetraphenylporphyrin (TPP) (**6**) as the porphyrin complex [49]. **6** was reacted first with pyridine and then silicon tetrachloride was added [49]. The reaction was then diluted with toluene and washed with hydrochloric acid [49]. The product was chromatographed and underwent crystallization in toluene and methanol to collect the product (TPP)$Si(OMe)_2$ (**6-Si(OMe)$_2$**) [49]. This product was then reacted with NaOH in THF to produce (TPP)$Si(OH)_2$ (**6-Si(OH)$_2$**) [49]. Following these new reaction conditions, it is common for the hydrolysis step to occur in the presence of different additives or solvents, including KOH, water, or MeOH (Fig. 7) [48,50–53].

#### 2.1.2. Lithium salt intermediate and use of hydrochlorosilanes

In 1995, Lemke et al. investigated new procedures to access (Por)$SiCl_2$ using tetra-*p*-tolylporphyrin (TTP) (**18**) as the base porphyrin [25]. The silylated product was not observed when Gouterman's method was applied; it was noted that under these acidic conditions the product was very water sensitive and prone to demetallation, which led to the protonated porphyrin $[(TTP)H_4]Cl_2$ instead [25]. Lemke et al. explored several pathways, including reacting (TTP)$[Li_2(THF)_2]$ (**9-[Li$_2$(THF)$_2$]**) with tetrachlorosilane, alkyl chlorosilanes, and hydrochlorosilanes [25]. The use of hydrochlorosilanes was the only successful method [25]. Upon this discovery, Lemke et al. developed a new one-pot synthetic route to access PorSils from free porphyrins; $(TTP)^{2-}$ is formed and reacted with $HSiCl_3$ or $H_2SiCl_2$ to form (TTP)$SiCl_2$ (**9-SiCl$_2$**) (Fig. 8) [25]. They observed that **9-SiCl$_2$** was extremely water-sensitive in solution (forming $[(TTP)H_4]Cl_2$), but could be exposed to atmospheric moisture briefly in solid form [25]. Reacting **9-[Li$_2$(THF)$_2$]** with $MeSiHCl_2$ or $Me_2SiHCl$ gives **9-SiMeCl** or **9-SiMe$_2$**, respectively [25].

Lemke et al. identified that (OEP)$SiCl_2$ (**2-SiCl$_2$**) is insensitive to moisture and is stable, unlike other (Por)$SiCl_2$ (i.e. Por = TPP(**6**), TTP (**9**), or TTFP (**13**)) acted in their hands [31]. Therefore, the Gouterman method works well to make **2-SiCl$_2$** because the product can endure the aqueous workup [31]. The difference in hydrolytic stability of porphyrin silane dichlorides of **9** (TTP) and **2** (OEP) were attributed to electronics [31]. Lemke et al. found their method to be broadly higher yielding than Gouterman's method; therefore, the procedure by Lemke et al. is more useful for the synthesis of (Por)$SiCl_2$ regardless of the porphyrin backbone [31].

In 2015, Remello et al. altered the formation of (Por)$Si(OH)_2$ by first conducting a three-step – lithiation, silylation, and dechlorination (Fig. 9) – single-pot synthesis to isolate a triflate (OTf) intermediate [31,54,20]. This intermediate was then hydrolyzed using NaOH to produce (Por)$Si(OH)_2$ [54]. The completion of each step was monitored by UV–Vis spectroscopy due to high sensitivity of porphyrin Soret and Q-bands to axial substitution [54,20,55].

#### 2.1.3. Use of Trichlorosilane and Triethylamine

In 2013, Liu et al. followed a modified method to form a PorSil, which does not involve the formation of the (Por)$[Li_2(THF)_2]$ intermediate. The base porphyrin was added to dichloromethane, then trichlorosilane and tripropylamine were added (Fig. 10) [56]. The product was purified through column chromatography on silica gel [56].

Work from our lab (Hussein et al.) involved the synthesis of PorSils following an approach similar to to Liu et al.; however, in our

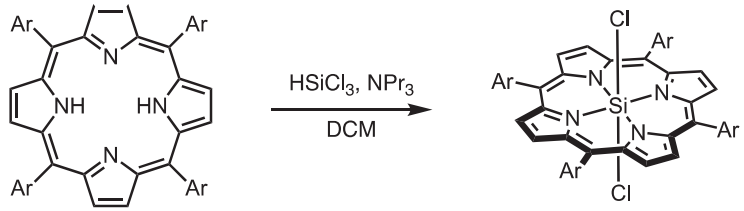


**6** Ar = Ph, TPP
**14** Ar = *p*-($C_{18}H_{15}N$)-Ph, TPAP

**6-SiCl$_2$** Ar = Ph, (TPP)$SiCl_2$
**14-SiCl$_2$** Ar = *p*-($C_{18}H_{15}N$)-Ph, (TPAP)$SiCl_2$

**Fig. 10. Synthesis of (Por)$SiCl_2$ by Liu et al.** Adapted method from Lemke et al., in which the lithium intermediate is not applied, and triethylamine is used as the base.

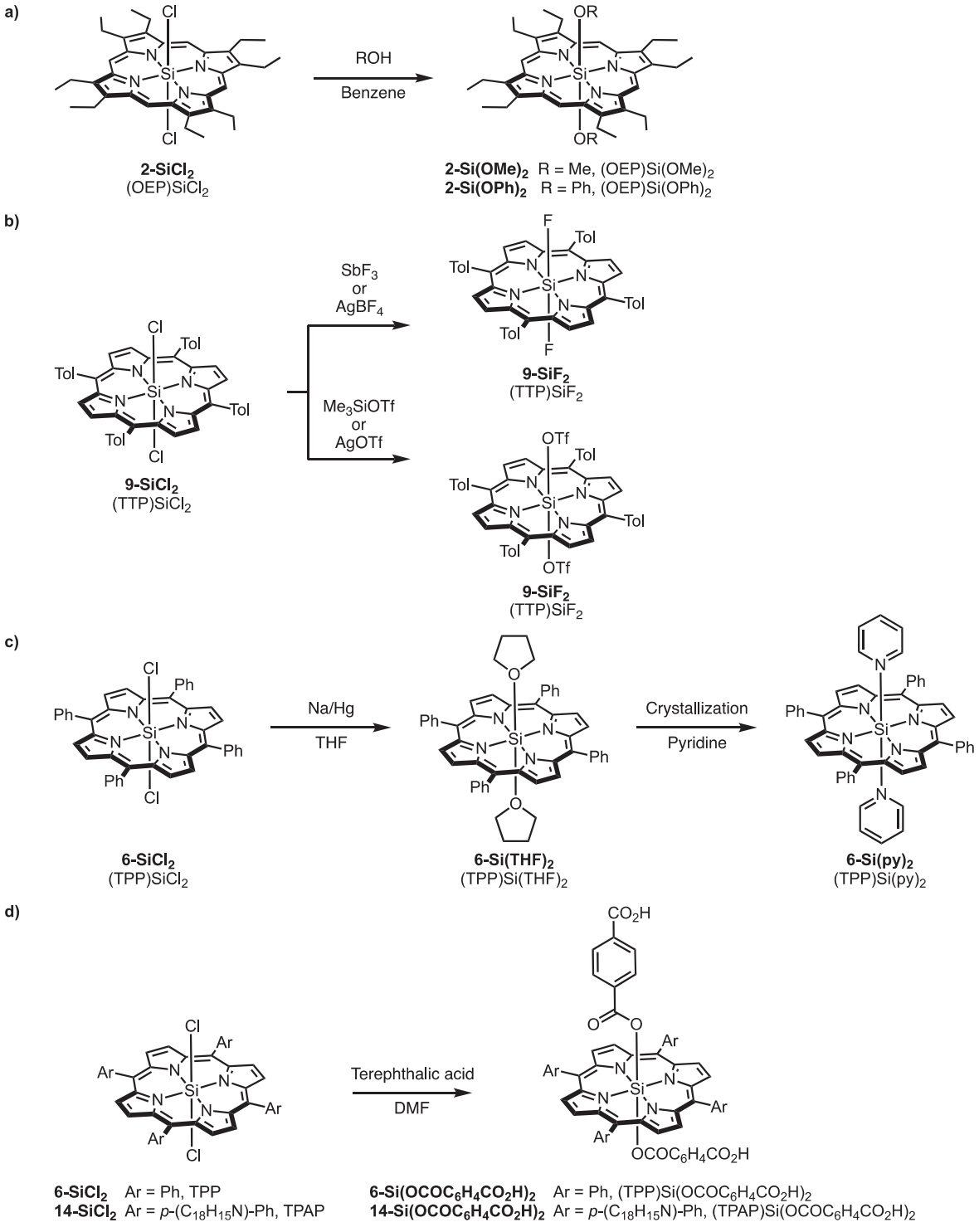


**Fig. 11. Derivatization of Various (Por)$SiCl_2$ Building Blocks. a)** Installation of an alkoxy and aryloxy group, **b)** Fluorination and triflation, **c)** Synthesis of a PorSil with THF and pyridine axial ligands via reduction, **d)** Installation of carboxylate axial ligands.

hands column chromatography of the (Por)$SiCl_2$ was not successful [57]. We silylated the base porphyrin through the addition of trichlorosilane and triethylamine; following an aqueous workup, the triethylamine was removed by evaporation and the product was isolated [57]. The (Por)$SiCl_2$ was transformed to the (Por)Si$(OH)_2$ building block via refluxing in THF and water [57].

### *2.2. Derivatization and reactivity of porphyrin silanes*

The (Por)$SiCl_2$ and (Por)$Si(OH)_2$ building blocks can be derivatized by introducing axial substituents on the silicon center. Axial substituents can vary based on sterics or electronics; their nature can alter the reactivity of the porphyrin complex, either through

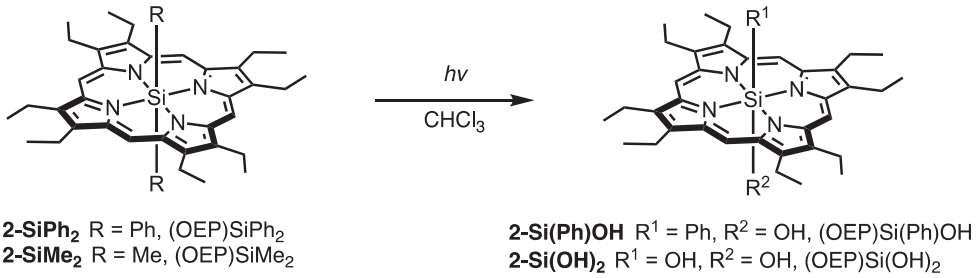


**Fig. 12. Derivatization of PorSil via Photolysis**. The PorSils, **2-SiPh$_2$** and **2-SiMe$_2$** behave differently under the same photolysis reaction conditions, producing **2-Si(Ph)OH** and **2-Si(OH)$_2$** respectively.

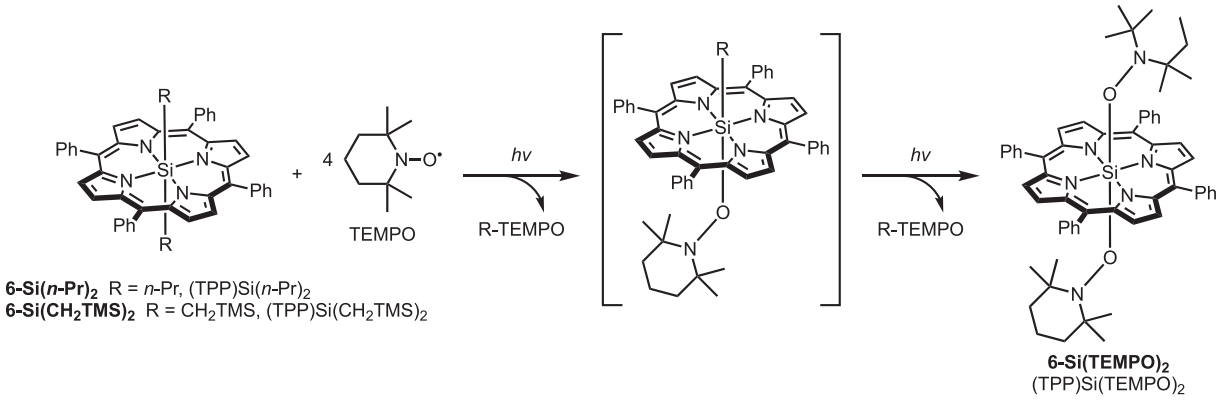


**Fig. 13. Irradiation of Dialkyl PorSils in the Presence of Nitroxy Compounds.**Irradiating (greater than420 nm) solutions of either **6-Si(*n*-Pr)$_2$** or **6-Si(CH$_2$TMS)$_2$** in separate NMR tubes with TEMPO gave **6-Si(TEMPO)$_2$** quantitatively, also generating two equivalents of (*n*-Pr)TEMPO or (CH$_2$TMS)TEMPO, respectively.

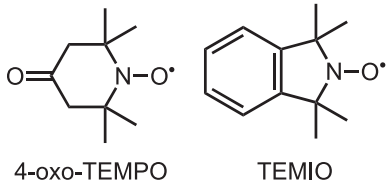


**Fig. 14. Structures of 4-oxo-TEMPO and TEMIO.** These radical scavengers can be applied to follow the same reaction procedure seen in Fig. 8 to produce **6-Si(4-oxo-TEMPO)$_2$** and **6-Si(TEMIO)$_2$**.

derivatization of the silicon center or, in the case of (Por)Si(OH)$_2$, functionalization at the axial oxygen atom.

### 2.2.1. Derivatization of the silicon center

Derivatization at the silicon center generally involves the heterolytic dissociation of an axial Si-X bond, where X is Cl, OMe, or OTf – and subsequent attack by a nucleophile, which can include alkoxy, phenoxy, alkyl, aryl, and carboxy groups. Additionally, photochemistry and electrochemistry have been explored to derivatize the silicon center.

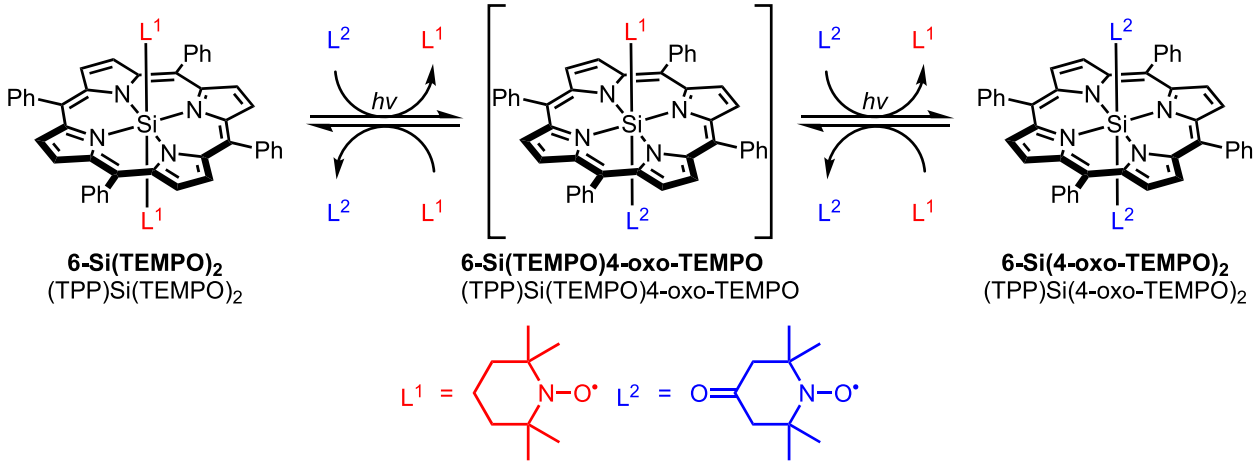


**Fig. 15. Ligand Exchange via Photolysis.** Dinitroxy PorSils (**6-Si(TEMPO)$_2$** and **6-Si(4-oxo-TEMPO)$_2$**) underwent ligand exchange in the presence of free dinitroxy compounds and light.

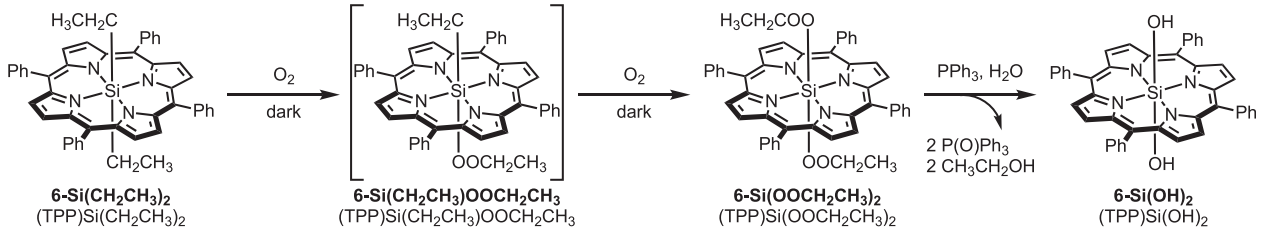


**Fig. 16. Peroxidation, Reduction, and Hydrolysis of a Dialkyl PorSil.** The two axial ligands are peroxidized stepwise, as evidenced by the gradual appearance and disappearance of **6-Si(CH$_2$CH$_3$)OOCH$_2$CH$_3$** over 25 days, peaking at 11 days. Reduction of **6-Si(OOCH2CH$_3$)$_2$** with PPh$_3$ gives **6-Si(OCH$_2$CH$_3$)$_2$** which is then hydrolyzed to **6-Si(OH)$_2$** by H$_2$O.

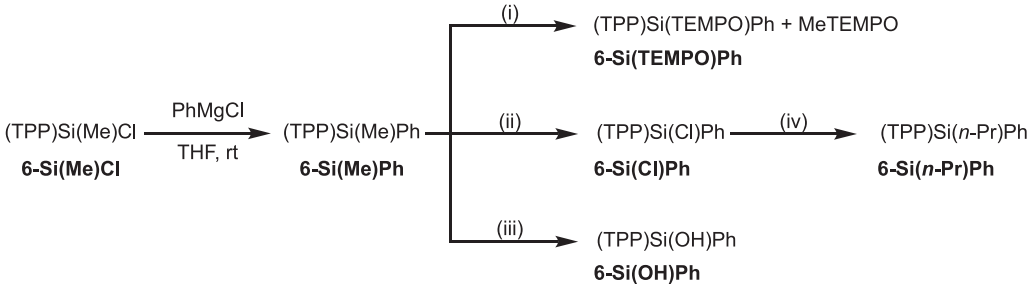


**Fig. 17. Photolysis and Oxidation Reactions by Ishida et al.** (i) h$\nu$ (7 min), TEMPO, $C_6D_6$, (ii) hv (10 min), $CCl_4$, (iii) TCNQ, DCM, (iv) *n*-PrMgBr, THF.

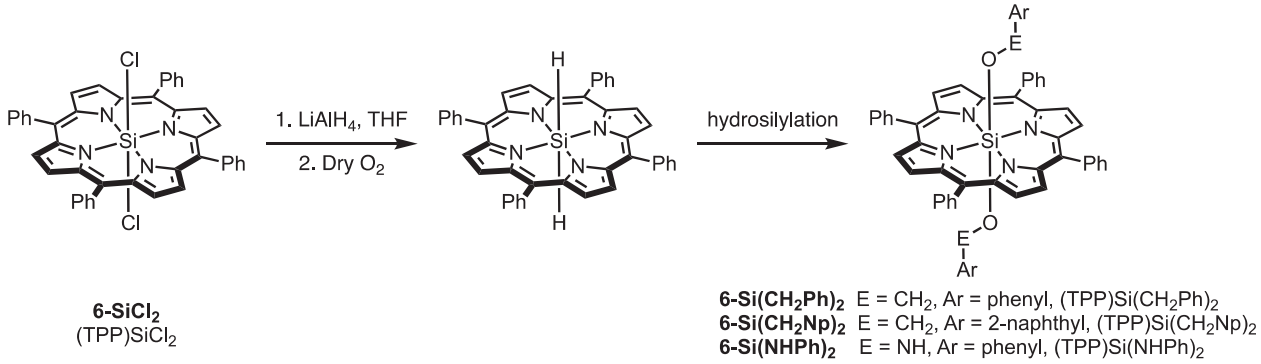


**Fig. 18. Synthesis and Reactions of (TPP)SiH$_2$. 6-SiH$_2$** was produced when **6-SiCl$_2$** was exposed to LiAlH$_4$ in THF, followed by O$_2$. Hydrosilylation of benzaldehyde, 2-naphthaldehyde, or nitrosobenzene was conducted by exposure to **6-SiH$_2$** in THF to yield **6-Si(CH$_2$Ph)$_2$**, **6-Si(CH$_2$Np)$_2$**, or **6-Si(NHPh)$_2$**, respectively. [62]

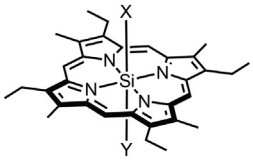


| Name | X | Y |
|---|---|---|
| **1-Si(OH)$_2$** | OH | Y = X |
| **1-Si(OSi(Me)$_3$)$_2$** | OSi(CH$_3$)$_3$ | Y = X |
| **1-Si(OEt)$_2$** | OCH$_2$CH$_3$ | Y = X |
| **1-Si(OSi(OEt)$_3$)OH** | OSi(OCH$_2$CH$_3$)$_3$ | OH |
| **1-Si(OSi(OEt)$_3$)OSiMe$_3$** | OSi(OCH$_2$CH$_3$)$_3$ | OSi(CH$_3$)$_3$ |
| **1-Si(OSi(OEt)$_3$)$_2$** | OSi(OCH$_2$CH$_3$)$_3$ | Y = X |
| **1-Si(OSiOtBu(OEt)$_2$)$_2$** | OSiOC(CH$_3$)$_3$(OCH$_2$CH$_3$)$_2$ | Y = X |
| **1-Si(OSi(OtBu)$_2$OEt)$_2$** | OSi(OC(CH$_3$)$_3$)$_2$OCH$_2$CH$_3$ | Y = X |
| **1-Si(OSi(OtBu)$_2$OH)$_2$** | OSi(OC(CH$_3$)$_3$)$_2$OH | Y = X |
| **1-Si(OSi(OtBu)$_2$OSi(Me)$_3$)$_2$** | OSi(OC(CH$_3$)$_3$)$_2$OSi(CH$_3$)$_3$ | Y = X |
| **1-Si(OSi(OtBu)$_3$)$_2$** | OSi(OC(CH$_3$)$_3$)$_3$ | Y = X |

**Fig. 19. (Etio-I)Si Derivatives.** Several (Etio-I)Si derivatives were synthesized by Boylan and Calvin.

There have been several reports of PorSil derivatization from the (Por)SiCl$_2$ building block. (OEP)SiCl$_2$ (**2-SiCl$_2$**) was transformed to **2-Si(OMe)$_2$** and **2-Si(OPh)$_2$** through the addition of methanol for the former and phenol in benzene for the latter (Fig. 11a) [42]. (TTP)SiCl$_2$ (**9-SiCl$_2$**) can be fluorinated to **9-SiF$_2$** using SbF$_3$ or AgBF$_4$, as well as triflated to **9-Si(OTf)$_2$** using Me$_3$SiOTf or AgOTf (Fig. 11b) [25]. A reduction of (TPP)SiCl$_2$ (**6-SiCl$_2$**) was conducted by adding two equivalents of Na/Hg in THF to yield **6-Si(THF)$_2$** [35]. This product was then subjected to crystallization from hexanes and dissolved in pyridine, which produced **6-Si(py)$_2$** (Fig. 11c) [35]. **6-SiCl$_2$** and (TPAP)SiCl$_2$ (**14-SiCl$_2$**) were derivatized to form PorSils with carboxylate axial substituents; in this case, the building block was reacted with terephthalic acid in DMF to produce a disubstituted terephthalate PorSil (Fig. 11d) [56].

Grignard chemistry has been applied for the derivatization of the silicon center to generate PorSils bearing C-ligated axial sub-

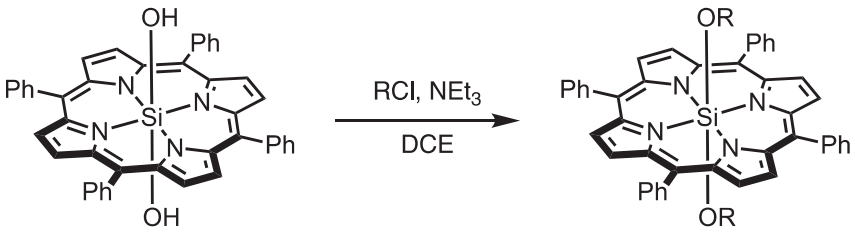


**6-Si(OH)$_2$**
(TPP)Si(OH)$_2$

| Name | R |
|---|---|
| **6-Si(OSiEt$_3$)$_2$** | SiEt$_3$ |
| **6-Si(OSi$^i$Pr$_3$)$_2$** | Si$^i$Pr$_3$ |
| **6-Si(OSi$^i$BuMe)$_2$** | Si$^i$BuMe$_2$ |
| **6-Si(OSiBu$_3$)$_2$** | SiBu$_3$ |
| **6-Si(OSiHex$_3$)$_2$** | SiHex$_3$ |
| **6-Si(OSiPhMe$_2$)$_2$** | SiPhMe$_2$ |
| **6-Si(OSiPh$_2$Me)$_2$** | SiPh$_2$Me |
| **6-Si(OSiPh$_2$Bu)$_2$** | SiPh$_2$Bu |
| **6-Si(OSiPh$_3$)$_2$** | SiPh$_3$ |

**Fig. 20. Bissilyloxy PorSils.** Compound **6-Si(OH)$_2$** was reacted with a chlorosilane (RCl) and triethylamine in DCE in order to produce (TPP)Si(R)$_2$. [57]

stituents [22–23,58]. The Grignard reagent RMgBr can be added to (Por)SiCl$_2$ to form (Por)SiR$_2$, where R represents Me, Ph, *n*-Pr, CH$_2$-TMS, C$_6$H$_5$, CH = CH$_2$, and C≡CC$_6$H$_5$ [58–59]. (TPP)-SiMePh (**6-SiMePh**) was also produced using Grignard chemistry by reacting PhMgBr with **6-SiMeCl** in THF [22]. (TTP)SiF$_2$ (**9-SiF$_2$**) readily reacts with strong nucleophiles like PhLi and MeMgBr to produce **9-SiMe$_2$** or **9-SiPh$_2$**, respectively [22,60]. This is interesting because *cis* hexacoordinated silicon compounds have no reaction with strong nucleophiles, while having almost identical Si-halide bond lengths seen in PorSils [60]. Therefore, the reactivity in nucleophilic substitution observed for **9-SiF$_2$** may be attributed to its *trans* geometry [60].

Derivatization of the silicon center via photolysis has also been explored. Kadish et al. explored light-assisted selective hydrolysis of (OEP)SiPh$_2$ (**2-SiPh$_2$**) and **2-SiMe$_2$** [23]. The exposure of a CHCl$_3$ solution of **2-SiPh$_2$** to visible light for one day produced **2-Si(Ph)OH**, while **2-SiMe$_2$** was converted to **2-Si(OH)$_2$** under the same conditions (Fig. 12) [23].

Zheng et al. reported photochemical reactions of organosilicon porphyrins with radical scavengers and highlighted the formation of a long-lived silicon diradical. Irradiation of dialkylsilicon porphyrins with visible light in the presence of nitroxy compounds produced the dinitroxide complex **6-Si(TEMPO)$_2$** seen in Fig. 13. This reaction did not proceed in the dark, which indicated the critical aspect of visible light [33].

(TPP)Si(4-oxo-TEMPO)$_2$ (**6-Si(4-oxo-TEMPO)$_2$**) and (TPP)Si(TEMIO)$_2$ (**6- Si(TEMIO)$_2$**) complexes were obtained from reactions analogous to those seen in Fig. 13, but with 4-oxo-TEMPO and TEMIO traps (Fig. 14).

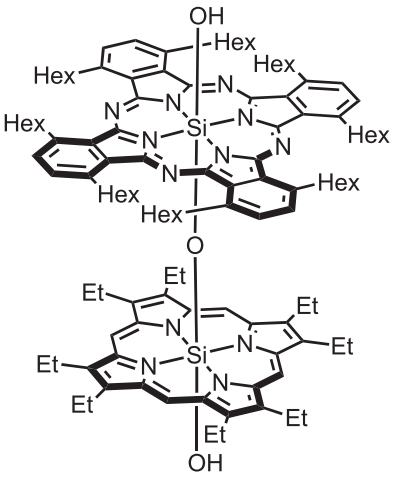


**15**

**Fig. 21. $\mu$-oxo Linked Phthalocyanine-Porphyrin Dyad.** The dimer was synthesized by reacting **2-Si(OH)$_2$** with dihydroxy silicon octakis(hexyl)phthalocyanine in pyridine.

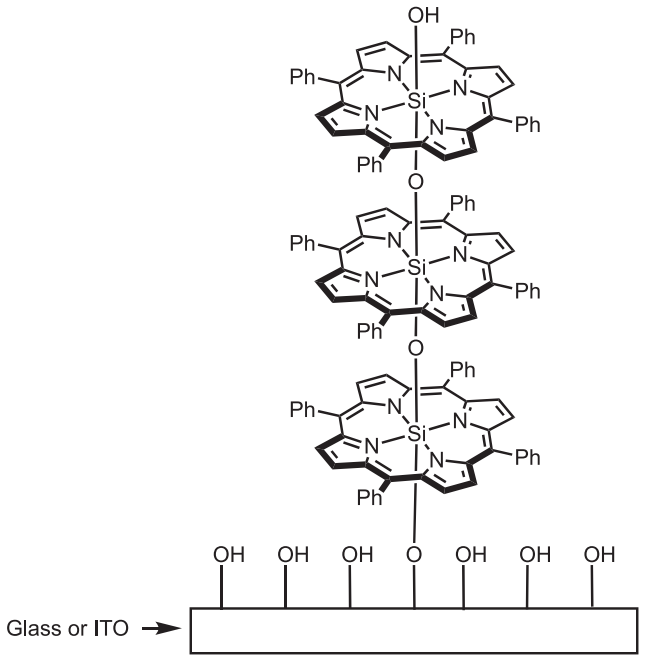


**Fig. 22. Multilayer Porphyrin Assembly.** A layer-by-layer approach was used to assemble a porphyrin siloxane oligomer in a controlled fashion on a glass or ITO plate.66.

This experiment indicates that the axial Si-C bond is homolytically cleaved to generate a porphyrin-bound silyl radical, which is trapped by the nitroxy compound [33]. No reactivity was observed when the axial ligands were unsaturated aliphatic groups, due to the higher stability of alkyl radicals. The dinitroxy PorSils (**6-Si(TEMPO)$_2$** and **6-Si(4-oxo-TEMPO)$_2$**) underwent photolysis in the presence of free nitroxy compounds and ligand exchange was observed (Fig. 15; this experiment demonstrated reversibility, homolysis of the Si-O bond, and a competitive recombination of the silyl radical with the free nitroxy compounds [33].

Zheng et al. identified that dioxygen can be inserted into axial Si-C bonds of a PorSil in the dark via a consecutive process of peroxidation, reduction, and hydrolysis (Fig. 16). The same procedure was attempted with (TPP)Si(R)$_2$, where R = CH = CH$_2$, C$_6$H$_5$ (**6-Si(C$_6$H$_5$)$_2$**), and C≡CC$_6$H$_5$ (**6-Si(C≡CC$_6$H$_5$)$_2$**), but they were inert to dioxygen conditions [61].

Ishida et al. explored the photolytic and oxidative behaviours of (TPP)SiMePh (**6-SiMePh**) (Fig. 17). Irradiation of **6-SiMePh** in the presence of TEMPO produced **6-Si(TEMPO)Ph** and MeTEMPO quantitatively, while photolysis of **6-SiMePh** in CCl$_4$ gives only **6-**

**Si(Cl)Ph**, showing typical silyl radical character [22]. It was also observed that **6-Si(Cl)Ph** can be converted to **6-Si(*n*-Pr)Ph** with Grignard chemistry [22]. Reacting **6-SiMePh** with one equivalent of tetracyanoquinodimethane (TCNQ) in the dark forms **6-Si(OH)Ph** in 91% yield, while excess TCNQ furnishes 75% of **6-Si(OH)$_2$** [22]. One-electron oxidation of **6-SiMePh** in the presence of $H_2O$ can also selectively cleave axial Si-Me bonds, consistent with theoretically favored homolytic cleavage of Si-Me bonds over Si-Ph by 38 kcal/mol [22].

Ishida et al. also derivatized the silicon by synthesizing porphyrin silicon hydrides. (TPP)$SiCl_2$ (**6-SiCl$_2$**) was exposed to $LiAlH_4$ in THF, followed by exposure to dry $O_2$ in order to yield **6-SiH$_2$**. This product was further manipulated via hydrosilylation with the polar double bonds C = O and N = O to produce **6-Si(CH$_2$Ph)$_2$**, **6-Si(CH$_2$Np)$_2$**, **6-Si(NHPh)$_2$** (Fig. 18) [62].

*2.2.2. Functionalization of the axial oxygen atom*

In addition to derivatization at the silicon center, PorSils can be functionalized at the axial oxygen atom to produce various derivatives, such as PorSils with silyloxy and THF ligands. Boylan et al. reported the first synthesis of silyloxy PorSils from Etio-I porphyrins (Fig. 19) [21]. **1-Si(OSi(Me)$_3$)$_2$** was synthesized through a trimethylsilylation of **1-Si(OH)$_2$** with bis(trimethylsilyl)acetamide in pyridine [21,40]. Compounds **1-Si(OEt)$_2$**, **1-Si(OSi(OEt)$_3$)OH**, **1-Si(OSi(OEt)$_3$)$_2$**, **1-Si(OSiOtBu(OEt)$_2$)$_2$**, **1-Si(OSi(OtBu)$_2$OEt)$_2$**, **1-Si(OSi(OtBu)$_2$OH)$_2$**, and **1-Si(OSi(OtBu)$_3$)$_2$** were isolated from a mixture of products when **1-Si(OH)$_2$** is treated with ethyl or t-butyl alcohol [21]. Trimethylsilylation of **1-Si(OSi(OEt)$_3$)OH** and **1-Si(OSi(OtBu)$_2$OH)$_2$** produced **1-Si(OSi(OEt)$_3$)OSiMe$_3$** and **1-Si(OSi(OtBu)$_2$OSi(Me)$_3$)$_2$**, respectively [21].

Trimethylsilylation and *tert*-butyldimethylsilylation of axial hydroxy groups were carried out with various PorSils including (Etio-I)Si(OH)$_2$ (**1-Si(OH)$_2$**), (OEP)Si(OH)$_2$ (**2-Si(OH)$_2$**), (Etio-III)Si(OH)$_2$ (**3-Si(OH)$_2$**), and (OMP)Si(OH)$_2$ (**4-Si(OH)$_2$**) [44]. Trimethylsilylation was conducted using *N*,*N*-bis(trimethylsilyl)trifluoroacetamide to form (Por)Si(OTMS)$_2$, while *tert*-butyldimethylsilylation was performed using *tert*-butyldimethylchlorosilane and imidazole to make (Por)Si(OTBDMS)$_2$ [63,44,64,47]. In 1984, Marriot et al. updated the silylation procedure to form the (Por)Si(OTBDMS)$_2$ complex using Corey's reagent (i.e. *N*-methyl-*N*-(*tert*-butyldimethylsilyl)trifluoroacetamide) in pyridine [45–47,50]. We (Hussein et al.) functionalized the axial oxygen to synthesize a variety of bissilyloxy PorSils from TPP (**6**) (Fig. 20) [57].

Lemke et al. explored the functionalization of the oxygen atom by replacing triflate axial ligands with THF ligands. This was done by heating a solution of (OEP)Si(OTf)$_2$ (**2-Si(OTf)$_2$**) in THF at 50 °C for two hours. As a result, the complexes **[2-Si(OTf)(THF)](OTf)** or **[2-Si(THF)$_2$](OTf)$_2$** were observed in rapid equilibrium. The formation of silicon tetraarylporphyrin triflate (TArP)Si(OTf)$_2$ occurs in a unique way; THF solutions of (TArP)Si(OTf)$_2$ solidify in less than 12 h due to the polymerization of THF. Therefore, the displacement results in a Lewis acidic silyl cation, which initiates the ring opening polymerization (ROP) of THF. A longer time period (i.e. one month) is required for such a phenomenon to occur with **2-Si(OTf)$_2$**. This duration is influenced by the electronic properties of the porphyrin backbone: **2** is electron rich, which reduces the electrophilicity of silicon and promotes the dissociation of triflate. The resulting silyl cation is not a strong enough Lewis acid to promote ROP of THF. The TArP backbone is less electron rich, which increases the electrophilicity of silicon and binds the triflate groups more tightly [31].

Zhao et al. produced a $\mu$-oxo linked phthalocyanine-porphyrin dyad through functionalization of the axial oxygen atom (Fig. 21) [65]. This occurred by reacting (OEP)Si(OH)$_2$ (**2-Si(OH)$_2$**) with dihydroxy silicon octakis(hexyl)phthalocyanine in pyridine. [65] The production of this dyad was confirmed by mass spectroscopy of the crude product; however, attempted isolation of the product by column chromatography was unsuccessful [65].

Lee et al. introduced a layer-by-layer approach to transform the (TPP)$SiCl_2$ (**6-SiCl$_2$**) monomer into a multilayer of cofacially aligned porphyrins. The multilayer is linked through the axial oxygen atoms by selective siloxane formation (Fig. 22) [66]. The layers were assembled by a repeating process of dipping an indium tin oxide (ITO) plate in a solution of **6-SiCl$_2$**. [66]. Stepwise single porphyrin deposition was confirmed by observing that the intensity of the UV/Vis signal at the Soret band of the porphyrin was near-linearly correlated to the number of layers. The O-Si-O chains themselves were identified as physically linear (i.e. O-Si-O bond angle of 180°); some deviation was observed upon reaching a size of five or higher [66].

Kanaizuka et al. explored self-assembled monolayers of PorSils by conducting a one-pot continuous silane coupling reaction from (OEP)$SiCl_2$ (**2-SiCl$_2$**), which formed an uneven structure made of joined PorSils that they called "bamboo shoots". X-ray diffraction studies confirmed the periodic structure existed in layers, while electronic microscopy and X-ray crystallography identified needles of PorSils that were perpendicular and parallel to the glass/FTO substrate [67]. Chambers et al. addressed this problem of random orientation with the introduction of silicon tetrachloride and Si-O covalent bonding using **2-Si(OH)$_2$**. Colloidal lithography was applied to fabricate surface films and nanostructures with PorSils. A one-pot reaction was conducted where silicon tetrachloride was added to **2**, followed by hydrolysis and condensation to form the Si-O-Si bridges [68]. Baklanov et al. carried out the first on-surface synthesis of a non-metal porphyrin via thermal desorption, where atomic silicon was evaporated onto a free-base TPP layer on a Ag(100) surface under ultra-high vacuum conditions [69].

*2.2.3. Hydrolysis and methanolysis*

The hydrolysis and methanolysis of PorSils are affected by both the nature of the base porphyrin and the axial ligands. (OEP)$SiCl_2$ (**2-SiCl$_2$**) is less sensitive to moisture than tetraaryl PorSil dichlo-

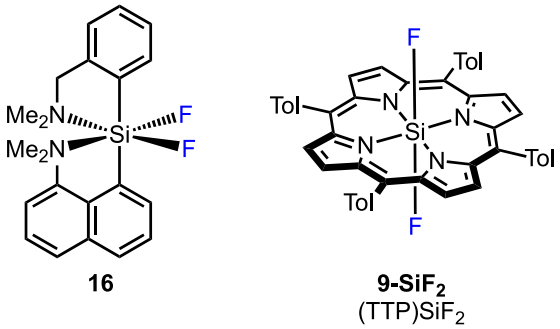


**Fig. 23. Geometry of PorSils.** *Cis* hexacoordinated silicon (left) compared to a *trans* hexacoordinated silicon (right) geometry observed in PorSils. [31,58,73]

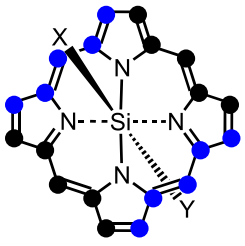


**Fig. 24. Ruffled Conformation of a General PorSil.** The blue and black circles represent the carbon atoms below the above and below the nitrogen plane, respectively. [58]

**Table 1**
Structural Data of Reported PorSil Crystal Structures.

| Compound | Δ r (Å)[a] | Si-X (Å) | Si-N (Å)[b] | Ref. |
|---|---|---|---|---|
| (TFPP)$SiF_2$ | 0.67 | 1.64 | 1.92 | [60] |
| 13-$SiF_2$ | | | | |
| (TTP)$SiF_2$ | 0.63 | 1.64 | 1.92 | [60] |
| 9-$SiF_2$ | | | | |
| (TTP)$Si(O_3SCF_3)_2$ | 0.79 | 1.842(4) | 1.87 | [25,60] |
| 9-$Si(O_3SCF_3)_2$ | | 1.821(4) | | |
| (TPP)$Si(CH_2Si(CH_3)_3)_2$ | 0.09 | 1.929(6) | 2.01 | [58] |
| 6-$Si(CH_2Si(CH_3)_3)_2$ | | | | |
| (TPP)$Si(CH=CH_2)_2$ | 0.03 | 1.83(2) | 2.01 | [58] |
| 6-$Si(CH=CH_2)_2$ | | | | |
| (TPP)$Si(C_6H_5)_2$ | 0.48 | 1.943(4) | 1.97 | [58] |
| 6-$Si(C_6H_5)_2$ | | 1.950(3) | | |
| (TPP)$Si(C{\equiv}CC_6H_5)_2$ | 0.13 | 1.819(2) | 1.98 | [58] |
| 6-$Si(C{\equiv}CC_6H_5)_2$ | | | | |
| (TPP)$Si(OSiPhMe_2)_2$ | 0.469 | 1.688(2) | 1.96 | [57] |
| 6-$Si(OSiPhMe_2)_2$ | | 1.681(2) | | |
| (TPP)$Si(OSiPh_2Me)_2$ | 0.006 | 1.6758(14) | 1.98 | [57] |
| 6-$Si(OSiPh_2Me)_2$ | | | | |
| (TPP)$Si(OSiPh_2{}^tBu)_2$ | 0.111 | 1.6801(12) | 1.98 | [57] |
| 6-$Si(OSiPh_2{}^tBu)_2$ | | | | |
| (TPP)$Si(OSiPh_3)_2$ | 0.058, 0.085[b] | 1.684(3) | 1.98 | [57] |
| 6-$Si(OSiPh_3)_2$ | | 1.690(3)[c] | 1.98 | |
| (TPP)$SiH_2$ | 0.582 | 1.47(2) | 1.9654(17) | [62] |
| 6-$SiH_2$ | | | | |
| (TPP)$Si(THF)_2$ | 1.00 | 1.891 | 1.844 | [35] |
| 6-$Si(THF)_2$ | | | | |

[a] Δ r represents the average displacement of the *meso* carbon atoms from the pyrrole 4 N plane.
[b] The indicated Si-N values are an average of the lengths of the four Si-N bonds, which may or may not be equivalent to each other in a given structure.
[c] Two Δ r values are assigned because the compound contains an asymmetric unit that has two conformational poses.

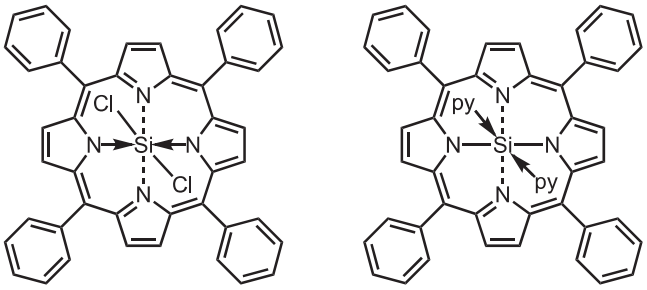


**6-$SiCl_2$**
(TPP)$SiCl_2$

**6-Si(py)$_2$**
(TPP)Si(py)$_2$

**Fig. 25. Electronic Structures of the Aromatic 6-$SiCl_2$ and Antiaromatic 6-Si(py)$_2$.** [34] Aromatic PorSils demonstrate electronic distribution between the nitrogen atoms and central silicon. On the contrary, antiaromatic PorSils demonstrate electronic distribution between the axial ligands and silicon, which leads to a more ruffled geometry.

rides [31]. The methanolysis of (TTP)$SiCl_2$ (**9-$SiCl_2$**) forms the monosubstituted **9-Si(OMe)Cl**. (TTFP)$SiCl_2$ (**13-$SiCl_2$**) contains the least electron-donating porphyrin backbone of known tetrarylporphyrin silanes and readily reacts with MeOH to form a 1:1 mixture of the mono- and disubstituted complexes [25,31].

PorSils with fluoride axial ligands are stable and unreactive with water or methanol [43,31]. Water sensitive PorSils, such as (TTP)$Si(OTf)_2$ (**9-Si(OTf)$_2$**) and ($C_{12}$TPP)$Si(OMe)_2$ (**7-Si(OMe)$_2$**), hydrolyze to PorSils with dihydroxy axial ligands [25,53]. For PorSils with the OEP (**2**) or Etio-I (**1** backbone, the OTBDMS axial ligands demonstrate greater stability to solvolysis compared to the OTMS axial ligands; [45] notably, it is likely that the O-(TMS/TBDMS) bond is hydrolyzing as opposed to the O-(central silicon) bond in this case. The OTBDMS ligand also has greater temperature stability; in gas chromatography, the TMS derivative experiences degradation at temperatures above 200 °C, whereas OTBDMS is more stable to flash volatilisation [45]. It is hypothesized that (Por)Si$(OTBDMS)_2$ is more stable to thermolysis and solvolysis due to increased steric bulk [64].

#### 2.2.4. Dissociation of silicon

Demetallation does not typically occur for (Por)Si$(OH)_2$ at room temperature. However, when a solution of (TPP)Si$(OH)_2$ (**6-Si(OH)$_2$**) was heated in sulfuric acid, dissociation was observed (Eq. (1)) [51].

$$(OH)_2SiTPP - - - H^{+Solv} + 3H^{+Solv} \xrightarrow{H_2SO_4} H_4TPP(SO_3H)_x^{2+} + (OH)^2Si_{Solv}^{2+} \quad (1)$$

In comparison to lead, tin, and germanium TPP complexes, (TPP)Si$(OH)_2$ (**6-Si(OH)$_2$**) was measured to be the least kinetically stable in acidic conditions. This stability is influenced by the strength of the M−N sigma bonds. The small size of the silicon atom leads to radial compression of the macrocycle and decreases the covalent contribution to the Si-N bonds, which explains the low kinetic stability of **6-Si(OH)$_2$** under these conditions [51,70,71].

## 3. Properties of PorSils

### 3.1. Structural and physical properties

#### 3.1.1. Geometric considerations and planarity

The geometry of PorSils has been investigated using X-ray crystallography (Table 1) and computational methods. These investigations have provided information on the isomerism, planarity, bond lengths, and bond angles of PorSils [25,57,35,58,60,34,72]. Hexacoordinate silicon complexes are typically *cis*-coordinated with respect to labile, highly electronegative substituents. On the contrary, the axial ligands of all reported PorSils' crystal structures necessarily demonstrate a *trans* orientation (Fig. 23), regardless

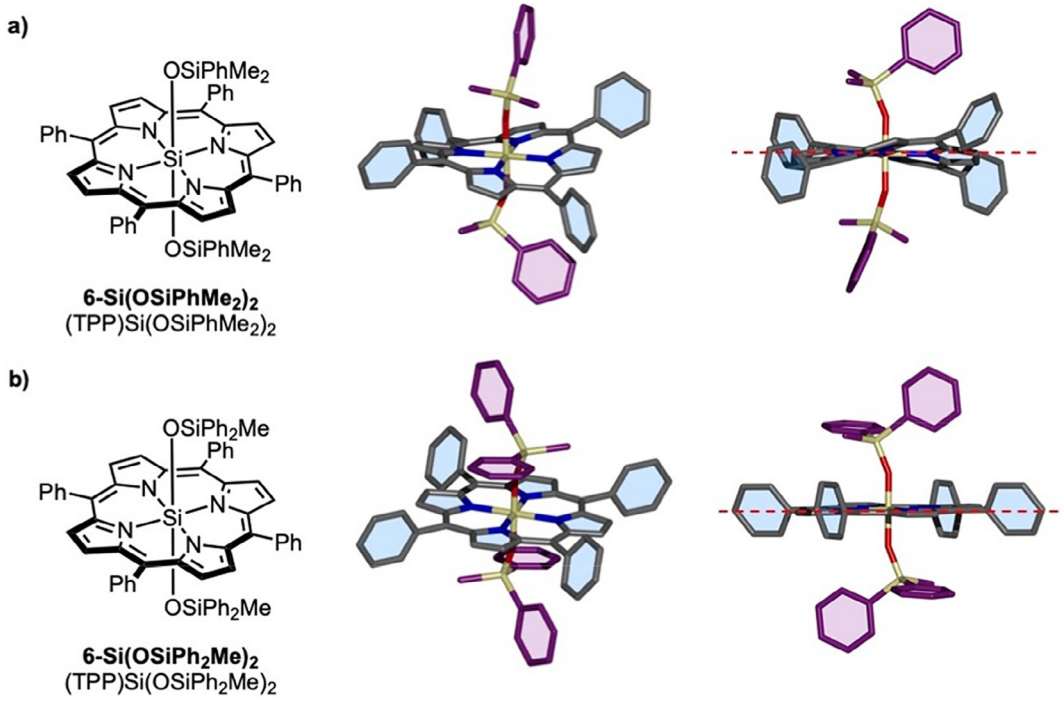


**Fig. 26. Examples of Crystal Structures of PorSils.** [57] X-ray crystal structures of a) **6-Si(OSiPhMe$_2$)$_2$**, which shows high degree of ruffling, and b) **6-Si(OSiPh$_2$Me)$_2$**, which is nearly completely planar.

of identity [25,35,57–58,60]. The bond angle between the central silicon and axial ligands are also reportedly linear [25,57].

PorSils are expected to be non-planar due to the small size of the central silicon. Aida et al. explained that the electron-donating or electron-withdrawing capacity of the axial substituent impacts the planarity of PorSils [58]. We (Hussein et al.) outlined that planarity of a PorSil can be achieved if i) the axial substituents are small enough that they do not interfere with the porphyrin and ii) the axial substituent is able to provide the silicon with extra electron density through π-back bonding, which lengthens the Si-N bond [57]. The compound (TPP)Si(OSiMePh$_2$)$_2$ (**6-Si(OSiMePh$_2$)$_2$**) is reported as the most planar PorSil to date, as the *meso* carbons *trans* to each other are displaced above and below the plane by +/- 0.011 Å [57]. Extended Hückel calculations predict that the minimum M−N distance for a porphyrin macrocycle to adapt a planar conformation is 1.90 Å, while any bond length over 2.01 Å is non-planar [74–75]. Non-planar conformations of porphyrins include ruffled, saddled, domed, and waved [76,77]. Most PorSils demonstrate a ruffled conformation (Fig. 24; ruffling is characterized by the displacement of the *meso* substituents, which lead to a twisting of the pyrrole rings [25,58,60,77]. Despite the ruffling configuration of the *meso* substituents and pyrrole rings, the nitrogen atoms and the silicon are understood to be coplanar [25,77].

Nonlocal density functional theory (DFT) demonstrated that the presence of axial ligands in PorSils can increase the electron density donated to the central metal, which allows for greater flexibility compared to other metalloporphyrins and lower ruffling torsion angles [76]. The degree of ruffling observed in PorSils differs based on the nature of the axial ligands, ranging from nearly planar to a *meso* carbon displacement (Δr) of 1.0 Å (Table 1). Antiaromatic PorSils (i.e. (TPP)Si(THF)$_2$ (**6-Si(THF)$_2$**) and **6-Si(py)$_2$**) are highly ruffled compared to aromatic PorSils due to the electron density distribution to the silicon (Fig. 25) [33,34].

Fluoride-containing ligands, such as (Por)SiF$_2$ and (Por)Si(OTf)$_2$, demonstrate a ruffling of the porphyrin ring and a saddle shape around the central silicon [25,58,60,78]. For TTP (**9**) and TTFP (**13**) complexes, identical Si-F bond distances were observed as 1.64 Å. This distance is similar to what is seen in *cis*-difluoro hexacoordinate silanes, suggesting that a *trans* configuration has no impact on Si-F bond length. Furthermore, the identity of the *meso* substituent of the porphyrin (i.e. tolyl in **18** or trifluoromethylphenyl in **23**) does not impact the axial Si-F distance [60]. The bond length of Si-O of **9-Si(OTf)$_2$** is longer than Si-F and accordingly its Si-N bond length was shorter than that of the (Por)SiF$_2$ compounds [60]. The silicon in **9-Si(OTf)$_2$** has a greater positive charge due to triflate's greater electron withdrawing capability, which results in a larger Si-N interaction and a more ruffled geometry [58,60]. The fluoride ligands participate as a π-donor to the silicon, which decreases the positive charge of the silicon and leads to a more planar geometry compared to the triflated PorSil [60]. A less ruffled geometry was observed for PorSils with the electron-donating ligands, such as CH = CH$_2$ and C$_6$H$_5$ [58]. **6-Si[CH$_2$Si(CH$_3$)$_3$]$_2$** and **6-Si(C≡CC$_6$H$_5$)$_2$** also diverge from the typical ruffled geometry, as they are nearly planar but with a slightly "waved" chair-like conformation [58]. The structural data from all reported crystal structures of PorSils are categorized in Table 1, and some images of a family of silyloxy porphyrin silanes can be seen in Fig. 26.

When comparing aliphatic ligands with differing "s" character, it was observed that Si-C bond lengths are shorter for $sp^2$- and *sp*-hybridized substituents than those bonded through $sp^3$-hybridized carbons. In addition to aliphatic ligands, the Si-C bond length for aryl axial ligands were studied and were determined to be longer than that of a vinyl ligand. This is attributed to steric interactions between the *ortho* hydrogens of the aryl group and the porphyrin ring. Besides the elongation of the Si-C bond length, PorSils with aryl axial ligands ruffle in order to minimize the these steric interactions [17,58,76].

The symmetry of PorSils has been studied and reported as an additional class of geometric and structural characterization. Various symmetries and point group assignments have been identified

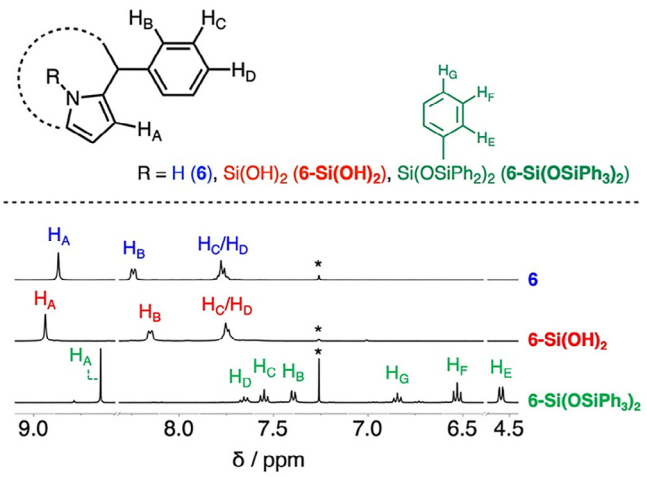


**Fig. 27. Examples of PorSil NMR Spectra.** [57] Partial $^1$H NMR spectra (400 MHz, $CDCl_3$, 298 K) of **TPPH$_2$**, **6-Si(OH)$_2$**, and **6-Si(OSiPh3)$_3$** showing (i) that aromatic resonances of the axial substituent are shifted upfield by their proximity to the porphyrin ring and (ii) that $H_B$ is shifted significantly upfield in aromatic SOPS (**1i**). *Signal from residual $CHCl_3$ in $CDCl_3$.

for specific PorSils. A DFT study was conducted by Liao and Scheiner to investigate the symmetry of a general PorSil, where the porphyrin backbone does not contain *meso* or axial substituents [79]. In this study, the PorSil has two extra electrons, which causes the silicon to move out of the plane by 0.77 Å and allows the symmetry to transition from a planar $D_{4h}$ symmetry to a distorted $C_{4v}$ symmetry [79]. DFT calculations were also carried out by Vangberg and Ghosh for (Por)$SiCl_2$ and (Por)$SiF_2$, where the porphyrin backbone does not contain *meso* substituents. These compounds demonstrated $D_{4h}$ symmetry [76]. $D_{4h}$ symmetry was also observed for (Por)Si$(OH)_2$ through Hückel calculations conducted by Gouterman and Schaffer [74]. Kane and Lemke investigated the symmetry of (TTP)Si$(OTf)_2$ (**9-Si(OTf)$_2$**from its crystal structure; the compound demonstrates a point group symmetry of $C_{2v}$ and a localized symmetry of $D_{2d}$, which is required to accommodate small central atoms [25].

### 3.1.2. Volatility

Prior to 1964, gas chromatography was not useful for porphyrin separations due to their low volatility [21,44]. This issue was addressed by the production of the novel PorSils by Boylan and Calvin. The introduction of bulky trialkylsilyloxy axial substituents increased the volatility of porphyrins because the axial ligands reduce π-π stacking [21,40,44]. The addition of each OTMS axial group allows for an increase in volatility and a decrease in retention volume compared to porphyrins with divalent metal centers. This was particularly observed when comparing (Etio-I)Si$(OTMS)_2$ (**1-Si(OTMS)$_2$**) and **1-Ni**, which have molecular weights of 682 and 534, respectively [44]. Therefore, the presence of axial ligands has a greater impact on volatility than molecular weight [44]. It is understood that the large axial groups prevent intermolecular interactions and adsorption in the capillary column, allowing for an decreased retention time [44].

The volatility of various fluoride-containing PorSils was studied in order to understand the effect of different fluoride axial ligands. Mono-fluorinated **1-Si(OTMS)(F)** has a longer retention time than (Por)Si$(OTMS)_2$, which could be due to the localized dipole charge across the Si-F bond [44]. The OTBDMS PorSil derivative demonstrated greater thermal and solvolytic stability as well as longer retention times compared to the OTMS derivative, making it a more favourable compound for GC–MS [45–46,64,80]. Bulky OTBDMS groups further increase the volatility presumably due to reduced aggregation effects [50]. However, it was noted that additional bulkiness does not increase volatility, but volatility does vary with molecular weight [21]. Evershed et al. stated that different axial ligands do not affect fragmentation, but the strength of the bond between the metal and the ligand affects the intensity of the peak [64]. Overall, the fragmentation of the PorSils observed in the mass spectra often depicted the loss of one or both of the axial ligands [21,40,44,45,47,63,64].

### 3.1.3. Solubility

Silylated porphyrins generally had improved solubility when compared to other metalloporphyrins [25]. (Por)$SiCl_2$ and (Por)$SiF_2$ complexes have good solubility in organic solvents. However, solubility can differ based on the porphyrin backbone; for example, PorSils with octaethyl backbones are less soluble than those with tetraaryl backbones [31]. Unlike the dichloro and difluoro variants, (OEP)Si$(OTf)_2$ (**2-Si(OTf)$_2$** dissolves readily in THF; this however is accompanied by spontaneous reaction with the solvent [31]. In addition to organic solvents, (TCPP)Si$(OH)_2$ (**10-Si(OH)$_2$**) was identified to be water soluble, while (TPyP)Si$(OH)_2$ (**12-Si(OH)$_2$**) is almost insoluble in water [54,55].

The effect of axial ligands on the solubility of PorSils was pointedly examined with silyloxy PorSils [57]. Such compounds are less prone to aggregation and therefore have a greater solubility than their base porphyrin, TPP (**6**) [57]. Silyloxy PorSils with aromatic axial ligands are generally more soluble than those with aliphatic axial ligands [57]. A Hirschfeld plot demonstrated that PorSils interact at distances that correspond to the sum of their Van der Waals radii, which minimizes aggregation and thus increases solubility [57].

### 3.1.4. Mesomorphic properties

PorSils can be mesogenic, meaning their molecular coordination complexes exhibit liquid crystalline properties [53,81]. DSC measurements were conducted and it was determined that ($C_{12}$TPP)Si$(OH)_2$ (**7-Si(OH)$_2$**) have two phase transitions (84 °C and 211 °C), where the first corresponds to the melting of the solid and the second represents iotropization [52,53]. X-ray measurements elucidated that the mesophase depicts a lamellar type ordering, also known as smectic type of ordering [53]. A 3D plastic lamellar mesophase with a columnar structure and a face-to-face arrangement was observed, where the axial hydrogens are connected by a weak hydrogen bond, demonstrated by IR spectroscopy at varying temperatures [52]. The hydrogen bonding allows for stabilization, which leads to the wider temperature range for the phase transitions compared to other metalloporphyrins [52]. The compound **7-Si(OCH$_3$)$_2$** is very hygroscopic making it difficult to study its mesomorphic properties [53]. A lamellar mesophase was also observed for the (TPP)Si$(OH)_2$ (**6-Si(OH)$_2$**) [82].

## 3.2. Electronic and spectral properties

### 3.2.1. NMR analysis

The aromatic macrocyclic porphyrin possesses a ring current that shields the axial substituent protons and shifts them upfield in an NMR spectrum (Fig. 27). This effect is less prominent for protons further from the porphyrin center; for example, the *ortho* protons on the axial phenyl group of (TPP)Si$(OSiPh_3)_2$ (**6-Si(OSiPh$_3$)$_2$**) experience a great amount of shielding and their NMR signal is seen at 4.69 ppm, whereas the *meta* protons are less shielded and so their NMR signal is closer to the aromatic region at 6.57 ppm. Interestingly, the signals of the *meta* and *para* protons of the *meso* phenyl ring are well-resolved in the **6-Si(OSiPh$_3$)$_2$** spectrum, which is not observed for the free TPP complex or the other silyloxy PorSils synthesized by Hussein et al. [57] This indicates that the magnetic effects of the axial phenyl groups is strong

enough to influence the peripheral phenyl groups and that electronic information can be transmitted between these two groups.

*3.2.2. Redox activity*

Many biological redox systems use metal complexes, such as metalloporphyrins, as reaction centers [83,84]. The redox activity of the porphyrin ring is influenced by the nature of the central metal, planarity, the *meso* substituents, and any present axial ligands [78,85]. It has been proposed that silicon porphyrins are harder to reduce than tin and germanium porphyrins due to the small size of the silicon center and a decrease in planarity of the porphyrin ring [78,85]. Ruffling of the porphyrin interferes with the conjugation of the porphyrin π-system, ultimately affecting its ability to be reduced [78]. An increase in porphyrin planarity can lead to an increase in ring reduction because the interaction of the d-π metal-ring orbitals increases [78,85]. Computational testing was carried out by Kang et al. for (Por)$SiCl_2$ (i.e. Por = TPP (**6**), TMP (**11**), and TFPP (**13**)) and comparisons were made to zinc porphyrins. It was calculated that ruffled PorSils have higher LUMO energies and lower electron affinity values, which lead to increased electron injection and transport. However, the electron affinity for PorSils is greater when compared to zinc porphyrins with the same porphyrin backbone [77]. The larger electron affinity indicates that the ruffled geometry of PorSils have a greater ability to extract electrons [77].

A comprehensive table of published cyclic votammetry data for PorSils can be seen in Table 2 in the Appendix. The nature of the axial ligand can have a strong effect on the compound's redox activity. A more electron-rich axial ligand has a stronger Si-X bond and longer Si-N bond, which eases the ruffled geometry and allows for an easier reduction [78]. An increase in redox activity is seen with an increase in electronegativity of the axial ligand; the electron density of the silicon lowers with a highly electronegative ligand, enabling the π system of the ring to readily gain electrons during the reduction process [78,85]. Therefore, when comparing the ligands $F^-$, $Cl^-$, and $OTf^-$, the species containing the most electronegative ligand, being the fluoride, is the easiest to reduce [78].

It has been noted that the both reduction and oxidation of PorSils occur only through the porphyrin ring. Redox activity at the silicon centre is not observed due to its stability to electrochemical oxidation or reduction [83,85]. Porphyrin rings have demonstrated reversible oxidation in two one-electron steps, yielding π cation radicals and dications, as well as reduction in two reversible steps, yielding π anion radicals and dianions [78,83]. However, the number of redox processes and their potential(s) can vary between different PorSils. For example, silyloxy PorSils can undergo a reversible one-electron oxidation and reduction [57]. Each of silyloxy PorSils demonstrate a greater reduction potential than both its base porphyrin and porphyrin building block [57]. The cofacial porphyrin multilayers (Fig. 22) produced an oxidation half wave nearly identical to the (TPP)$SiCl_2$ (**6-SiCl$_2$**) monomer, where a quasi-reversible first oxidation and irreversible second oxidation were observed [66]. A stable cyclic voltammetric response was observed for the multilayers, which indicates that the assembly is stable [66].

*3.2.3. Photophysical properties*

PorSils are known to demonstrate excellent photophysical properties, including higher quantum yields and longer fluorescence lifetimes than other metalloporphyrins (Table 2) [86]. The excitation of electrons from the HOMO to the LUMO in metalloporphyrins generally leads to the weak absorption band (Q-band) in the UV–Vis region and a strong band (B or Soret band) in the near UV region [79]. Molar extinction coefficients in the range of $10^3$ $M^{-1}$ $cm^{-1}$ are often related to these compounds [86]. The reported PorSils produce two to four Q-bands, where $Q_2$ is often the most intense Q band [57]. In reference to the (Por)$SiCl_2$ building block, the derivatized PorSils often demonstrate a 40-nm red shift of all absorption bands, depending on the electron withdrawing or donating abilities of the axial ligands [23,86]. It was also noted that an increase in ruffling can lead to a red-shift of both the Soret band and Q-bands of PorSils [87]. The presence of axial ligands has led to a reduction in intermolecular aggregation without negatively affecting the photophysical properties [56,86].

Porphyrins produce two emission bands in fluorescence spectroscopy, attributed to their two tautomeric states [57]. It has been noted that the environment of the PorSil, such as the solvent, can affect the population distribution of the two tautomers but not the energy of the HUMO-LUMO gaps. This is shown as the intensity of the fluorescent bands differs in varying solvents, but the wavelengths remain consistent [57]. The fluorescence bands of (TPP)$SiCl_2$ (**6-SiCl$_2$**) occur at 615 and 666 nm [34]. Derivatized silyloxy PorSils produce two emissions around 600 nm and 650 nm when excited at the wavelength of their Soret band [57]. This range demonstrates a blue shift from that of the base porphyrin, which is a similar behaviour to metalloporphyrins [57]. The building block, **6-Si(OH)$_2$**, demonstrates a unique behaviour as it produces three emission signals [57]. This may be due to an optical character that is a hybrid of the base porphyrin and metalloporphyrins, or it could be due to aggregation [57].

The fluorescence of (TPP)Si$(py)_2$ (**6-Si(py)$_2$**) is noticeably weaker than its building block and its lifetime is 750-fold shorter [34]. Therefore, internal conversion is much easier and faster for **6-Si(py)$_2$** than for **6-SiCl$_2$** [34]. This is due to 1) its distorted geometry and 2) the presence of one or more excited singlet states that lie below the Q excited state [34]. The first factor is due to the steric interactions from bulky pyridine substituents that lead to distortion, which correspond to weaker fluorescence and shorter excited-state lifetimes [34]. **6-Si(py)$_2$** was also subjected to a double reduction/oxidation, which resulted in a weak luminescence and short excited-state lifetime. These results were attributed to the rapid nonradiative decay present in the low-energy excited states of **6-Si(py)$_2$** that are not present in the building block [34].

## 4. Applications

*4.1. Volatile porphyrin silanes for GC/MS analysis*

Geoporphyrins and petroporphyrins are present in sediments and crude oils [50,80]. They represent the "molecular fossils" of chlorophylls, bacteriochlorophylls, and hemes in organisms [50]. These complex mixtures found in geological materials are best separated through powerful separation techniques, such as gas chromatography and combined GC–MS [40]. However, the structural determination of porphyrins from oil shale rocks, shale oils, and petroleum have been limited because of their low volatility [40,80,88]. Boylan and Calvin identified that the demetallation of the porphyrins followed by the insertion of silicon improves the compounds' volatility and allows for GC/MS analysis [21,40].

Silylation improved the isolation and characterization of petroporphyrins in three different sources of natural petroleum: Gilsonite bitumen, Boscan crude oil, and La Luna shale [40,45–46,63,80]. The use of (Por)Si$(OTBDMS)_2$ revealed 123 individual porphyrins with abundances greater or equal to 0.1% for the petroporphyrins of Gilsonite [46]. The (Por)Si$(OTBDMS)_2$ derivatives were also applied for the analysis of the Boscan crude oil and the La Luna shale, which are both derived from Maracaibo Basin samples [80]. These samples demonstrated five similar series of porphyrins, as well as a greater number of porphyrins with a higher degree of saturation compared to the Gilsonite [80]. The GC method technique for the analysis of alkyl porphyrin mixtures in

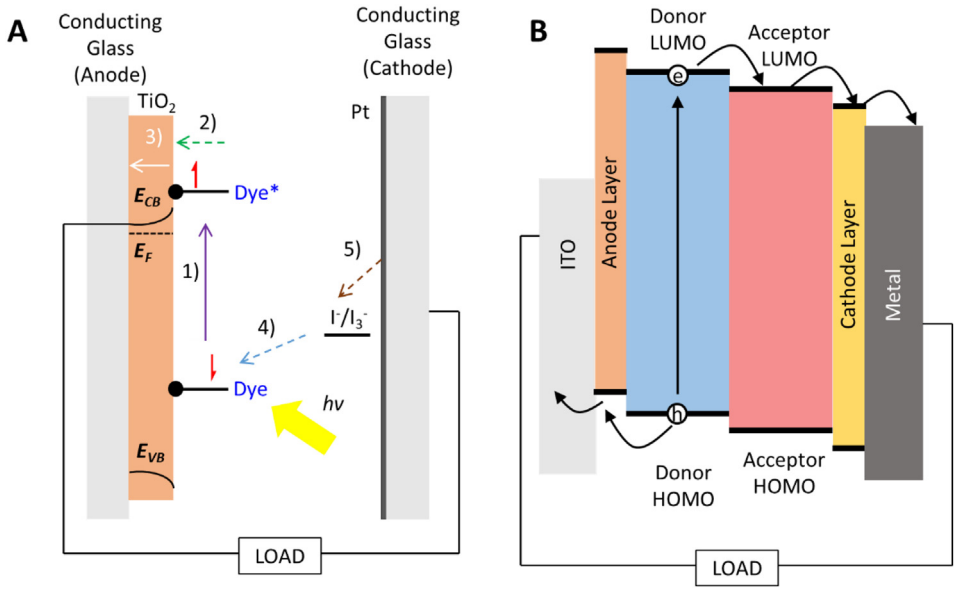


**Fig. 28. General Constructs of Light-Harvesting Technologies.** Schematic diagrams of **a)** a DSSC device) and **b)** an OPV. Porphyrins can be applied as the dye in a DSSC and as the acceptor in an OPV in order to convert solar energy into electrical energy.

Boscan crude oil was not commonly applied due to adsorption effects leading to poor sensitivity, as well as poor resolution [44,63]. The use of an "on-column" mode of injection and fused silica columns addressed decomposition and irreversible adsorption obstacles [63]. Overall, the silylation of petroporphyrins allow for the separation of mixtures found in ancient biogenetic deposits, which provides information on the distribution of porphyrins across various geologies [21,80].

### 4.2. Electric and photoelectric applications

#### 4.2.1. Use as a conductive medium

Porphyrin complexes are of interest for photoconductive applications because of their well-known semiconducting properties, as well as the mesogenic properties present in some PorSils [82]. The metalation of porphyrins allows for charge generation at the mesogen/electrode interface of an ITO cell [82]. The photoconductivity of $(C_{12}TPP)Si(OH)_2$ (**7-Si(OH)$_2$**) pressed between ITO plates was investigated [53]. The compound demonstrated unique rectification behaviour compared to nickel and vanadyl porphyrins; it produced a greater photocurrent when the negative electrode was illuminated, whereas the other compounds responded to the illumination of the positive electrode [82]. **7-Si(OH)$_2$** exhibits comparable mobility of the positive and negative charge, which suggests that the photoexcitation of the anode injects electrons and the illumination of the cathode injects a hole [82]. These observations differed from the metal-free compound, **7**, which does not display photoconductivity [53].

#### 4.2.2. Light-Harvesting arrays and organic photovoltaics

Porphyrins' optical, electrochemical, and photophysical properties have led to their application in light harvesting technologies such as dye-sensitized solar cells (DSSCs) and organic photovoltaics (OPVs) [89]. DSSCs and OPVs are known to convert solar energy into electrical energy (Fig. 28). A typical DSSC is composed of a dye, $TiO_2$ conduction band (CB), an anode, a cathode, and an electrolyte to act as a redox mediator [10]. Porphyrins have commonly been used as the dye [10]. Upon illumination, the electrons in the dye become excited and create an electric current as they move through the components of the device; the dye is regener-

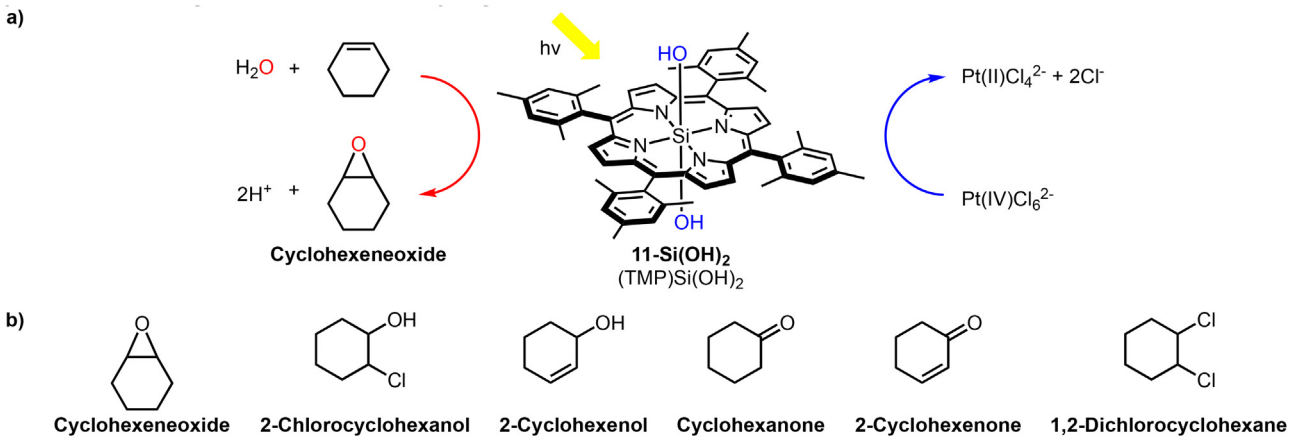


**Fig. 29. Photochemical Epoxidation of an Alkene.** In this system, water acts as an oxygen donor, $K_2PtCl_6$ is an electron acceptor, and a PorSil acts as the catalyst. The use of **11-Si(OH)$_2$** as the catalyst allows for the epoxidation of cyclohexene to form cyclohexeneoxide. [55]

ated by the redox mediator [10]. A typical OPV device contains an anode and cathode, as well as n-type acceptor and p-type donor materials. Porphyrins can be applied as acceptor materials, which withdraw and transport electrons, while the donor material donates electrons ($e^-$) and transports holes ($h^+$) [90]. An operational difference between OPVs and DSSCs is that electrons cycle within the host matrix of the latter without chemically changing it [53,91].

Liu et al. used PorSils with terephthalate axial ligands to anchor the dye to the $TiO_2$ surface in a DSSC. An "anchor" was applied to reduce the aggregation problems observed with porphyrin-based dyes on the $TiO_2$ surface. Both the terephthalate PorSil dyes examined (Fig. 11b) reduced molecular aggregation compared to a zinc porphyrin dye; however, the axial ligands led to a suppression of H-aggregates and a formation of J-aggregates. Dye **6-Si (OCOC$_6$H$_4$CO$_2$H)** exhibited poor photovoltaic performance, while **14-Si(OCOC$_6$H$_4$CO$_2$H)** demonstrated higher photocurrent and stronger light response at wavelengths greater than 400 nm. A larger charge transfer resistance was also observed with **14-Si (OCOC$_6$H$_4$CO$_2$H)**, which is due to the bulky peripheral groups that suppress electron recombination at the $TiO_2$/dye/electrolyte interface [56].

### 4.3. Dual luminophores for pressure/oxygen sensing

Polystyrene beads derivatized with luminescent dyes have a fast response to localized oxygen and have been used in biomedical applications [92,93]. These luminescent signals are strongly dependent on the experimental parameters, such as temperature, concentration, and light source [92]. The interactions between these variables were strengthened through the introduction of a dual luminophore, investigated by Im et al. [94] This dual luminophore system consists of (OEP)Si (**2-Si**) as a reference and **2-Pt** as an oxygen sensor [94]. The two luminophores were synthesized into polystyrene beads via dispersion polymerization [94]. The dual luminophores have similar absorption spectra but distinctive emission spectra; the silicon luminophore showed no response to oxygen, while the platinum was dependent on the concentration of oxygen [94]. Thus, this material allows for a self-referenced method to monitor the concentration of oxygen [94].

Luminophores made of ruthenium and platinum complexes have been applied to form pressure-sensitive paint (PSP), which is useful for unsteady aerodynamic applications [95]. Kimura et al. identified that there is no known method to provide a pressure field by measuring pressure globally and non-intrusively within a fluid flow; therefore, they applied their previously synthesized dual luminophore polystyrene beads to enable the global mapping of the pressure distribution within a fluid flow [95]. The film was stimulated at a common wavelength and it was observed that the silicon porphyrin did not change with concentration, but the platinum porphyrin intensity did decrease [95]. The intensity ratio of the two emissions allows for accurate measurement of pressure using airborne beads within the paint material [95].

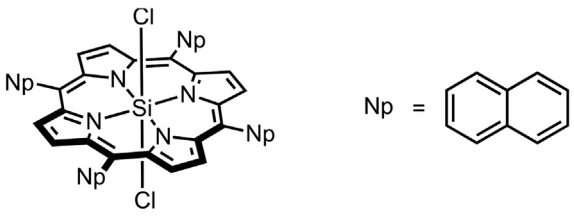


**17**
(TNP)SiCl$_2$

**Fig. 30. Structure of (TNP)SiCl$_2$ (17). 17** was investigated in addition to **6-SiCl$_2$** for its photodynamic therapy applications.

### 4.4. Photocatalysis

Metalloporphyrins have successfully been applied as photocatalysts in photochemical processes [20,96–101]. Artificial photosynthesis is a process of interest due to its application in biological modification, semiconductor photocatalysis, molecular catalysis, and system integration [54]. Artificial photosynthetic systems often face the "photon-flux density problem", which involves a four-step oxidation process to occur in order for a photon to be transferred [55]. This process requires a relatively lengthy timeframe of one second and the catalyst often experiences a transformation or decomposition before the next photon arrives [55]. PorSils are an attractive photocatalyst for these systems because silicon can exert a two-electron oxidation of water by one-photon excitation, which avoids the "photon-flux density problem" [54,55].

A visible-light-induced oxygenation of alkenes was tested using water as an oxygen atom donor, $K_2PtCl_6$ as an electron acceptor, and a PorSil as the catalyst [20]. This photoreaction takes advantage of the electrochemical properties of the PorSil, as the reaction proceeds under either the Q-band or Soret band excitation [20]. Remello et al. studied the following PorSils as catalysts for the photochemical epoxidation of cyclohexene: (TCPP)Si(OH)$_2$ (**8-Si(OH)$_2$**), (TMP)Si(OH)$_2$ (**11-Si(OH)$_2$**), (TFPP)Si(OH)$_2$ (**13-Si(OH)$_2$**) [20,55]. Photochemical epoxidation was only observed with **11-Si(OH)$_2$** as the catalyst due to its greater stability to the reaction conditions (Fig. 29a). The greater stability of **11-Si(OH)$_2$** compared **8-Si(OH)$_2$** and **13-Si(OH)$_2$** is attributed to its *ortho* methyl groups on the *meso* phenyl substituents, which protects the PorSil from nucleophilic attack of the chloride ion from $K_2PtCl_6$. The *ortho*-positions on the *meso* substituents of **8-Si(OH)$_2$** and **13-Si(OH)$_2$** are exposed to attack by the chloride ion, causing a hindrance of the oxygenated product, cyclohexeneoxide [55]. In addition to cyclohexeneoxide, a mixture of products were observed (Fig. 29b). The yield of each product changed based on varying concentrations of KOH in the reaction mixture [20].

A highly selective epoxidation was also observed with norbornene as the substrate, moderate results were seen with styrene, and no reaction was observed for 1-hexene. The reaction mechanism was investigated, and it was identified that the excited triplet state of the PorSil was responsible for the photochemical oxygenation. DFT calculations identified that an oxygen radical is formed on the axial ligand of the PorSil as a result of deprotonation. The radical undergoes an attack of the alkene, followed by an electron transfer to form the epoxide [55].

In addition to the oxygenation of alkenes by (TMP)Si(OH)$_2$ (**11-Si(OH)$_2$**) and (TpyP)Si(OH)$_2$ (**12-Si(OH)$_2$**) was also investigated by Remello et al. to conduct a two-electron oxidation of water to form hydrogen peroxide [54]. **12-Si(OH)$_2$** is a potentially attractive photocatalyst for due to the electron-withdrawing pyridines in the *meso* positions, which were expected to shift the oxidation of the PorSil to more positive values [54]. Electrolysis tests showed that an oxidation of **12-Si(O$^-$)$_2$** occurs, which forms **12-Si(O$^-$)(OOH)**. Water then undergoes a substitution with the hydroxide ligand to form hydrogen peroxide [54].

### 4.5. Photodynamic therapy

The interaction of light with biological systems is vital for important functions such as vision and photosynthesis, but it can also cause damage [102]. Damage can be mutagenic or carcinogenic; however, it can also be used in therapies [102]. Photodynamic therapy (PDT) is a non-invasive treatment that uses light

**Table 2**
**Comprehensive Data Summary of PorSils.** The table provides a summary of the cyclic voltammetry, absorption, and emission data of PorSils reported in literature.

| Compound | $E_{1/2}$ [eV] | | Absorption $\lambda_{max}$ [nm] | | Emission $\lambda_{max}$ [nm] | Ref. |
|---|---|---|---|---|---|---|
| | Oxidation | Reduction | Soret Bands ($\varepsilon \times 10^4$) | Q-Bands ($\varepsilon \times 10^4$) | | |
| (OEP)Si(OH)$_2$ | 0.92, 1.19[a,b] | −1.35[c] | – | – | – | 8, [83,84] |
| 2-Si(OH)$_2$ | 0.92, 1.39[e] | −1.43[e] | 389 (4.87), 407 (26.88)[d] | 471 (0.10), 536 (1.26), 572(1.38)[d] | | |
| (OEP)Si(Ph)OH | 0.86, 1.14, 1.16, 1.45[e] | −1.43[e] | 407 (5.29), 429 (19.25)[d] | 528 (0.34), 571 (1.60), 606 (0.24)[d] | - | [23] |
| 2-Si(Ph)OH | | | | | | |
| (OEP)SiPh$_2$ | 0.80, 1.15, 1.45[e] | −1.42[e] | 433 (5.93), 447 (27.19)[d] | 529 (0.32), 571 (1.58), 606 (0.26)[d] | - | [23] |
| 2-SiPh$_2$ | | | | | | |
| (OEP)SiMe$_2$ | 0.72, 1.12, 1.45[e] | −1.46[e] | 430 (8.24), 443 (29.12)[d] | 528 (0.34), 571 (1.60), 606 (0.24)[d] | - | [23] |
| 2-SiMe$_2$ | | | | | | |
| (OEP)Si(OMe)$_2$ | – | – | 408, 390, 337[f] | 573, 538, 502[f] | - | [23,42] |
| 2-SiOMe$_2$ | | | 430 (8.24), 443 (29.12)[d] | 528 (0.34), 571 (1.60), 606 (0.24)[d] | | |
| (OEP)Si(OPh)$_2$ | – | – | 408, 390, 337[f] | 573, 538, 505[f] | - | [42] |
| 2-Si(OPh)$_2$ | | | | | | |
| (OEP)SiF$_2$ | 0.977[g] | −1.444[g] | 388 (46.8)[h] | 508 (1.23), 542 (2.09)[h] | - | [31,78] |
| 2-SiF$_2$ | | | | | | |
| (OEP)SiCl$_2$ | 1.073, 1.463[g] | −1.614[g] | 385, 403[h] | 500, 534, 571[h] | - | [23,31,41,78] |
| 2-SiCl$_2$ | | | 388 (6.33), 408 (25.8)[d] | 502 (0.10), 537 (1.42), 575 (1.54)[d] | | |
| | | | 402 (18.6) | 520 (1.17), 550 (1.41)[i] | | |
| (OEP)Si(ClO$_4$)$_2$ | – | – | 403[c] | 539, 579[d] | - | [23] |
| 2-Si(ClO$_4$)$_2$ | | | | | | |
| (OEP)Si(O$_3$SCF$_3$)$_2$ | 1.103[g] | −1.291, −1.648[g] | 387 (19.4)[h] | 512 (0.56), 548 (1.38)[h] | - | [31,78] |
| 2-Si(O$_3$SCF$_3$)$_2$ | | | | | | |
| (Etio-I)Si(OH)$_2$ | – | – | 405 (31.4)[h] | 535 (11.7), 572 (13.8)[h] | - | [21] |
| 12-Si(OH)$_2$ | | | | | | |
| (TNP)SiCl$_2$ | – | – | 355 (1.4)[i] | 606 (1.0), 645 (1.0), 673 (2.5)[i] | 679[i] | [86] |
| 17 | | | | | | |
| (TFPP)SiF$_2$ | 1.358[g] | −1.056, −1.483[g] | 407 (61.7)[h] | 489 (0.23), 523 (2.29), 554 (0.27)[h] | – | [31,78] |
| 13-SiF$_2$ | | | | | | |
| (TFPP)SiCl$_2$ | 1.393[g] | −1.159, −1.615[g] | 429 (36.3)[h] | 492 (1.00), 535 (1.78), 571 (0.87)[h] | – | [31,78] |
| 13-SiCl$_2$ | | | | | | |
| (TTFP)Si(O$_3$SCF$_3$)$_2$ | 1.383[g] | −1.159 −1.660[g] | 407 (61.7)[h] | 490 (0.23), 523 (1.78), 556 (0.27)[h] | – | [31,78] |
| 13-Si(O$_3$SCF$_3$)$_2$ | | | | | | |
| (TTP)SiF$_2$ | 1.070, 1.504[g] | −1.245, −1.670[g] | 412 (32.4)[h] | 447 (0.81), 546 (1.38), 587 (0.40)[h] | – | [31,58,78] |
| 9-SiF$_2$ | | | | | | |
| (TTP)SiCl$_2$ | 1.161[g] | −1.357, −1.742[g] | 420 (33.8)[h] | 508 (0.29), 550 (1.10), 591 (0.40)[h] | – | [31,78] |
| 9-SiCl$_2$ | | | | | | |
| (TTP)Si(O$_3$SCF$_3$)$_2$ | 1.150, 1.363[g] | −1.354 −1.834[g] | 420 (55.0)[h] | 546 (2.10), 591 (0.66)[h] | – | [31,58,78] |
| 9-Si(O$_3$SCF$_3$)$_2$ | | | | | | |
| (TPAP)Si(OCOC$_6$H$_4$CO$_2$H)$_2$ | 0.96[k] | −0.84[k] | 411 (1.8), 452 (2.9)[j] | 572 (0.43), 600 (0.11)[j] | – | [56] |
| 14-Si(OCOC$_6$H$_4$CO$_2$H)$_2$ | | | | | | |
| (TPP)SiF$_2$ | 1.138, 1.553[g] | −1.245, −1.665[g] | 406 (46.8)[h] | 430 (2.24), 521 (1.66), 556 (3.89)[h] | – | [31,78] |
| 6-SiF$_2$ | | | | | | |
| (TPP)SiCl$_2$ | 1.176[g] | −1.386, −1.768[g] | 419 (38.0)[h] | 502 (0.30), 534 (1.35), 573 (0.50)[h] | – | [31,34,78,86] |
| 6-SiCl$_2$ | | | 437[l] | 530, 567, 611[l] | | |
| | | | 356 (0.40)[i] | 673 (1.7), 701 (1.1)[i] | | |
| (TPP)Si(O$_3$SCF$_3$)$_2$ | 1.202, 1.436[g] | −1.341, −1.705[g] | 408 (49.0)[h] | 523 (1.86), 554 (0.37)[h] | – | [31,78] |
| 6-Si(O$_3$SCF$_3$)$_2$ | | | | | | |

(*continued on next page*)

**Table 2** (*continued*)

| Compound | $E_{1/2}$ [eV] | | Absorption $\lambda_{max}$ [nm] | | Emission $\lambda_{max}$ [nm] | Ref. |
|---|---|---|---|---|---|---|
| | Oxidation | Reduction | Soret Bands ($\varepsilon \times 10^4$) | Q-Bands ($\varepsilon \times 10^4$) | | |
| $(TPP)Si(C_8H_5O_4)_2$<br>$6\text{-}Si(C_8H_5O_4)_2$ | 1.00[k] | −0.90[k] | 423 (3.2)[j] | 558 (0.18), 600 (0.11)[j] | – | [56] |
| $(TPP)Si(py)_2$<br>$6\text{-}Si(py)_2$ | – | – | 423[l] | 490, 529, 572[l] | – | [34] |
| $(TPP)Si(Pr)_2$<br>$6\text{-}Si(Pr)_2$ | – | – | 342.5, 425.5, 453.5[l] | 558, 608.5, 656[l] | – | [34] |
| $(TPP)Si(CH_2Si(CH_3)_3)_2$<br>$6\text{-}Si(CH_2Si(CH_3)_3)_2$ | – | – | 345.0, 454.5[l] | 562.0, 607.5, 654.5[l] | – | [34] |
| $(TPP)Si(CH=CH_2)_2$<br>$6\text{-}Si(CH=CH_2)_2$ | – | – | 340, 451[l] | 603, 648[l] | – | [34] |
| $(TPP)Si(C_6H_5)_2$<br>$6\text{-}Si(C_6H_5)_2$ | – | – | 343, 454.5[l] | 600, 645.5[l] | – | [34] |
| $(TPP)Si(C{\equiv}CC_6H_5)_2$<br>$6\text{-}Si(C{\equiv}CC_6H_5)_2$ | – | – | 329.5, 451[l] | 600, 645.5[l] | – | [34] |
| $(TPP)Si(OSiEt_3)_2$<br>$6\text{-}Si(OSiEt_3)_2$ | 1.33[m] | −1.06[m] | 421[h] | 513, 552, 589, 625[h] | 605, 643[h] | [57] |
| $(TPP)Si(OSi^iPr_3)_2$<br>$6\text{-}Si(OSi^iPr_3)_2$ | 1.36[m] | −1.21[m] | 422[h] | 512, 550, 591, 623[h] | 592, 627[h] | [57] |
| $(TPP)Si(OSi^tBuMe_2)_2$<br>$6\text{-}Si(OSi^tBuMe_2)_2$ | 1.34[m] | −1.08[m] | 418[h] | 512, 549, 586, 618[h] | 605, 646[h] | [57] |
| $(TPP)Si(OSiBu_3)_2$<br>$6\text{-}Si(OSiBu_3)_2$ | 1.32[m] | −1.18[m] | 424[h] | 514, 555, 596, 627[h] | 598, 645[h] | [57] |
| $(TPP)Si(OSiHex_3)_2$<br>$6\text{-}Si(OSiHex_3)_2$ | 1.32[m] | −1.35[m] | 423[h] | 514, 555, 595, 627[h] | 602, 649[h] | [57] |
| $(TPP)Si(OSiPhMe_2)_2$<br>$6\text{-}Si(OSiPhMe_2)_2$ | 1.35[m] | −1.10[m] | 423[h] | 514, 552, 591, 628[h] | 605, 649[h] | [57] |
| $(TPP)Si(OSiPh_2Me)_2$<br>$6\text{-}Si(OSiPh_2Me)_2$ | 1.36[m] | −1.08[m] | 422[h] | 514, 553, 592, 628[h] | 600, 648[h] | [57] |
| $(TPP)Si(OSiPh_2{}^tBu)_2$<br>$6\text{-}Si(OSiPh_2{}^tBu)_2$ | 1.35[m] | −1.11[m] | 423[h] | 512, 550, 587, 628[h] | 607, 648[h] | [57] |
| $(TPP)Si(OSiPh_3)_2$<br>$6\text{-}Si(OSiPh_3)_2$ | 1.33[m] | −1.13[m] | 425[h] | 515, 553, 592, 633[h] | 602, 645[g] | [57] |
| $(TPP)Si(OH)_2$<br>$6\text{-}Si(OH)_2$ | 1.52[m] | −0.93[m] | 410 (13.8)[n]<br>418[h]<br>446[h] | 524 (1.66), 571 (3.17), 612 (1.69), 652 (1.12)[n]<br>514[h]<br>550, 590, 649[h] | 600, 650, 711[g] | [51,57] |
| 5, 10, 15, triphenyl-20-p-phenoxy benzoic acid porphyrin silicon dichloride<br>$5\text{-}SiCl_2$ | – | – | 446[k] | – | – | [34] |

[a] The oxidation and reduction rates were calculated for this compound as $5*10^{-2}$ and $4*10^{-2}$ cm/s, respectively.
[b] The CV data was collected using a 0.01 M TBAP solution in $C_3H_7CN$.
[c] The CV data was collected using a 0.01 M TBAP solution in DMSO.
[d] The absorption data was collected by dissolving the compound in PhCN.
[e] The CV data was collected using a 0.1 M TBAP solution in PhCN.
[f] The absorption data was collected by dissolving the compound in benzene.
[g] The CV data was collected using a 0.1 M TBAP solution in DCM.
[h] The absorption data was collected by dissolving the compound in DCM.
[i] The absorption data was collected by dissolving the compound in DMSO.
[j] The absorption data was collected by dissolving the compound in THF.
[k] The CV data was collected in PhCN solutions and the dye loaded $TiO_2$ was applied as the working electrodes.
[l] The absorption data was collected by dissolving the compound in pyridine.
[m] The CV data was collected using 0.1 M $NBu_4PF_6$ solutions in DCM, with a scan speed of 100 mV $s^{-1}$, a temperature of 298 K, and referenced to a ferrocene ($[Fc]/[Fc]^+$) internal standard. Potentials are vs. NHE.
[n] The absorption data was collected by dissolving the compound in chloroform.

to release highly reactive species within the body on command [26,102–104]. When light and photosensitizers (PS) are in the presence of oxygen, they can yield locally destructive species, known as reactive oxygen species (ROS) (i.e. OH•, $O^{2-}$, and $^1O_2$) [104,105]. The efficacy of PDT depends in part on absorptivity of the PS beyond 630 nm where bodily tissues are most transparent to light [102,106,107].

Under photoirradiation, PorSils can generate ROS, which can lead to the cell death of tumoral cells [86]. For example, exposing the K562 tumor cell line to $(TPP)SiCl_2$ (**6-SiCl$_2$**) or $(TNP)SiCl_2$ (**17**, Fig. 30) and visible light showed low cell proliferation [86]. PorSils were also synthesized and conjugated to pluronic-silica (PluS) nanoparticles (NPs) and tested for their PDT activity on MCF-7 breast cancer cells [48]. 5,10,15-triphenyl-20-*p*-phenoxy benzoic

acid porphyrin silicon dichloride (**5-SiCl$_2$**) was used so that the peripheral carboxylic acid can join with the hydroxyl group of the PluS NPs to form an ester bond [48]. The cell vitality was decreased in the presence of **5-SiCl$_2$**, ultimately confirming the phototoxic behaviours of the PorSil [48].

## 5. Conclusion

This review highlights the importance and potential of PorSils. Since their discovery in 1967, synthetic methods to access them have evolved and a variety of PorSils have been synthesized. A wide range of axial substituents can be installed, which impact the physical and electronic properties of PorSils. Their structural, electronic, and photophysical properties have broadened the application scope of porphyrins; the uses of PorSils in the applications described in this review highlight the potential of PorSils.

From a broad perspective, one can make several statements regarding porphyrin silanes, and the impact of silylation and subsequent axial derivatization of porphyrins:

1. Dichlorosilylated porphyrins are readily synthetically accessible and this has been demonstrated with porphyrins possessing a range of $\beta$ and *meso* substituents. It is straightforward to subsequently convert the axial chlorides to substituents linked by another heteroatom – particularly oxygen-based substituents – or to alkyl/aryl groups via a polar substitution.
2. While labile axial substituents can be readily replaced under certain conditions (e.g. acidic or basic), they are generally resistant to hydrolysis/solvolysis even a) when the ligands are good leaving groups (e.g. Cl) and/or b) with extensive open-air handling in solution (i.e. column chromatography). Peripheral substitution affects reaction rates of substitution at the silicon center of the PorSil.
3. Photochemical substitution at the axial position of PorSils is also possible in certain cases.
4. The atomic radius of silicon is smaller than the central cavity in porphyrins, and therefore it is not uncommon to see highly ruffled porphyrins in PorSils. Planarity of these porphyrins can be modulated by axial substituents, and near-complete flattening has been observed.
5. Due to their three-dimensional nature, PorSils are generally less prone to aggregation than either non-metallated porphyrins or square-planar tetracoordinate metalloporphyrins. This renders PorSils both more volatile and more soluble than these other classes of porphyrins. The nature of the axial substituent affects these properties.
6. When PorSils are subjected to a magnetic field, axial substituents experience significant shielding by the aromatic porphyrin ring; this results in unique NMR profiles of these substituents.
7. PorSils display UV–Vis absorption profiles somewhere between free porphyrins and metalloporphyrins: while Q2 and Q3 are the largest Q-bands (like metalloporphyrins) Q1 and Q4 typically persisting (like free porphyrins). Axial substitution does not significantly impact $\lambda_{max}$ values, with the exception of OH, which may be due to intermolecular hydrogen bonding between the hydroxy axial substituents in solution.
8. The redox potential of PorSils is dependent on the identities of the axial substituents, with electronics playing an important role. For example, fluorinated PorSils tend to be easier to both reduce and oxidize than chlorinated PorSils. Stereoelectronic effects on redox potentials can be complex, as seen in the series of silyloxyporphyrin silanes (**6-Si(OSiR$_3$)$_2$**).

With respect to applications of PorSils, researchers have already identified many uses that take advantage of the above unique properties of these molecules. More widespread purposing of these molecules is expected now that a) synthetic routes are sufficiently accessible for research labs that are even only reasonably proficient in synthesis and b) there is a fuller understanding of the fundamental character of these molecules. In particular, we highlight the following potential applications where PorSils could make positive impact:

1. A less- or non-aggregating option to free porphyrin or square-planar tetracoordinate metalloporphyrin in a variety of applications where porphyrins are typically used, including in photovoltaics and as multipurpose dyes.
2. Novel siloxane polymers: polymers doped with PorSils may possess interesting properties and find use in a variety of fields.
3. Synthetic photosystems: axial ligation allows for the close associate of a porphyrin and another photosensitive molecule.
4. Molecular electronics: properties of extended conductive networks of porphyrins could be modulated, insulated, or linked by axial substituents.
5. Molecular switch relays: changing the properties of an axial substituent (i.e. conformation or electronics) could alter the properties of a PorSil (i.e. porphyrin planarity or redox potential).

We are hopeful that this review will serve as a resource and an inspiration for future work in this fertile field.

## Declaration of Competing Interest

The authors declare that they have no known competing financial interests or personal relationships that could have appeared to influence the work reported in this paper.

## Acknowledgements

The authors thank Ryerson University and NSERC for financial support of this work. The authors also thank Prof. Robert Gossage (Ryerson University) and Prof. Russell Viirre (Ryerson University) for helpful discussions, as well as Prof. Bryan Koivisto (Ryerson University) for additional support.

## Appendix

See Table 2

## References

[1] R. Giovannetti, The Use of Spectrophotometry UV-Vis for the Study of Porphyrins, Macro To Nano Spectrosc. (2012) 87–103, https://doi.org/10.5772/38797.
[2] U. Mazur, K.W. Hipps, A systematic approach toward designing functional ionic porphyrin crystalline materials, J. Phys. Chem. C. 112 (40) (2018) 22803–22820, https://doi.org/10.1021/acs.jpcc.8b03091.
[3] The Porphyrin Handbook; Kadish, K. M., Smith, K. M., Guilard, R., Eds.; 2000; Vol. 3. https://doi.org/10.1002/chin.200319291.
[4] P. Rothemund, A new porphyrin synthesis. the synthesis of porphin, J. Am. Chem. Soc. 58 (625–627) (1936).
[5] A.D. Adler, F.R. Longo, W. Shergalis, Mechanistic investigations of porphyrin syntheses. I. Preliminary studies on Ms-tetraphenylporphin, J. Am. Chem. Soc. 86 (15) (1964) 3145–3149, https://doi.org/10.1021/ja01069a035.
[6] A.D. Adler, F.R. Longo, J.D. Finarelli, J. Goldmacher, J. Assour, L. Korsakoff, A simplified synthesis for meso-tetraphenylporphin, J. Org. Chem. 32 (1) (1967) 476.
[7] T. Tanaka, A. Osuka, conjugated porphyrin arrays: synthesis, properties and applications for functional materials, Chem. Soc. Rev. 44 (4) (2015) 943–969, https://doi.org/10.1039/c3cs60443h.
[8] N.U. Day, C.C. Wamser, M.G. Walter, Porphyrin polymers and organic frameworks, Polym. Int. 64 (7) (2015) 833–857.
[9] J.L. Sessler, D. Seidel, Synthetic expanded porphyrin chemistry, Angew. Chemie - Int. Ed. 42 (42) (2003) 5134–5175, https://doi.org/10.1002/(ISSN)1521-377310.1002/anie.v42:4210.1002/anie.200200561.

[10] L.-L. Lu-Lin Li, E.-W.-G. Diau, Porphyrin-sensitized solar cells, Chem. Soc. Rev. 42 (1) (2013) 291–304.

[11] X. Xue, A. Lindstrom, Y. Li, Porphyrin-based nanomedicines for cancer treatment, Bioconjug. Chem. 30 (6) (2019) 1585–1603, https://doi.org/10.1021/acs.bioconjchem.9b00231.

[12] J.F. Lovell, C.S. Jin, E. Huynh, H. Jin, C. Kim, J.L. Rubinstein, W.C.W. Chan, W. Cao, L.V. Wang, G. Zheng, Porphysome nanovesicles generated by porphyrin bilayers for use as multimodal biophotonic contrast agents, Nat. Mater. 10 (4) (2011) 324–332, https://doi.org/10.1038/nmat2986.

[13] M. Overchuk, M. Zheng, M.A. Rajora, D.M. Charron, J. Chen, G. Zheng, Tailoring porphyrin conjugation for nanoassembly-driven phototheranostic properties, ACS Nano 13 (4) (2019) 4560–4571, https://doi.org/10.1021/acsnano.9b0049410.1021/acsnano.9b00494.s001.

[14] I. Beletskaya, V.S. Tyurin, A.Y. Tsivadze, R. Guilard, C. Stern, Supramolecular chemistry of metalloporphyrins, Chem. Rev. 109 (5) (2009) 1659–1713, https://doi.org/10.1021/cr800247a.

[15] S.J. Lee, J.T. Hupp, Porphyrin-containing molecular squares: design and applications, Coord. Chem. Rev. 250 (13–14) (2006) 1710–1723, https://doi.org/10.1016/j.ccr.2006.01.015.

[16] H. Ogoshi, T. Mizutani, Multifunctional and chiral porphyrins: model receptors for chiral recognition, Accounts Chem. Res. 31 (2) (1998) 81–89, https://doi.org/10.1021/ar9603165.

[17] P.J. Brothers, Recent developments in the coordination chemistry of porphyrin complexes containing non-metallic and semi-metallic elements, J. Porphyr. Phthalocyanines 6 (4) (2002) 259–267, https://doi.org/10.1142/S1088424602000294.

[18] J.E. Mark, Some interesting things about polysiloxanes, Acc. Chem. Res. 37 (12) (2004) 946–953, https://doi.org/10.1021/ar030279z.

[19] C. Battaglia, A. Cuevas, S. De Wolf, High-efficiency crystalline silicon solar cells: status and perspectives, Energy Environ. Sci. 9 (5) (2016) 1552–1576, https://doi.org/10.1039/c5ee03380b.

[20] S.N. Remello, T. Hirano, F. Kuttassery, Y. Nabetani, D. Yamamoto, S. Onuki, H. Tachibana, H. Inoue, Visible light induced oxygenation of alkenes with water sensitized by silicon-porphyrins with the second most earth-abundant element, J. Photochem. Photobiol. A Chem. 313 (2015) 176–183, https://doi.org/10.1016/j.jphotochem.2015.07.016.

[21] D.B. Boylan, M. Calvin, Volatile silicon complexes of etioporphyrin, J. Am. Chem. Soc. 89 (21) (1967) 5472–5473.

[22] S. Ishida, K. Yoshimura, H. Matsumoto, S. Kyushin, Selective Si–C bond cleavage on a diorganosilicon porphyrin complex bearing different axial ligands, Chem. Lett. 38 (4) (2009) 362–363.

[23] Kadish, K.M. Xu, Q.Y. Barbe, J.-M. Guilard, R. Synthesis and Reactivity of A-Bonded Silicon Metalloporphyrins. Spectroscopic Characterization and Electrochemistry. 1988, pp 1191–1.

[24] A.K. Pal, S. Varghese, D.B. Cordes, A.M.Z. Slawin, D.W. Ifor, E. Zysman-colman, Near-infrared fluorescence of silicon phthalocyanine carboxylate esters, Sci. Rep. (2017) 1–14, https://doi.org/10.1038/s41598-017-12374-8.

[25] K.M. Kane, F.R.P.J.L. Lemke, Bis(Trifluoromethanesulfonato)(Tetra-p-Tolylporphyrinato)Silicon(IV), (TTP)Si(OTf)2: The First Structurally Characterized (Porphyrinato)Silicon(IV) Complex, Inorg. Chem. 34 (16) (1995) 4085–4091.

[26] Y. Cheng, T.L. Doane, C.-H. Chuang, A. Ziady, C. Burda, Near infrared light-triggered drug generation and release from gold nanoparticle carriers for photodynamic therapy, Small 10 (9) (2014) 1799–1804, https://doi.org/10.1002/smll.v10.910.1002/smll.201303329.

[27] J. Li, Y. Yang, P. Zhang, J.R. Sounik, M.E. Kenney, Synthesis, Properties and Drug Potential of the Photosensitive Alkyl- and Alkylsiloxy-Ligated Silicon Phthalocyanine Pc 227, Photochem. Photobiol. Sci. 13 (12) (2014) 1690–1698, https://doi.org/10.1039/c4 pp00321g.

[28] E. Zysman-Colman, S.S. Ghosh, G. Xie, S. Varghese, M. Chowdhury, N. Sharma, D.B. Cordes, A.M.Z. Slawin, I.D.W. Samuel, Solution-Processable Silicon Phthalocyanines in Electroluminescent and Photovoltaic Devices, ACS Appl. Mater. Interfaces 8 (14) (2016) 9247–9253, https://doi.org/10.1021/acsami.5b1240810.1021/acsami.5b12408.s00110.1021/acsami.5b12408.s002.

[29] E. Palomares, M.V. Martínez-Díaz, S.A. Haque, T. Torres, J.R. Durrant, State Selective Electron Injection in Non-Aggregated Titanium Phthalocyanine Sensitised Nanocrystalline TiO2 Films, Chem. Commun. 18 (2004) 2112–2113, https://doi.org/10.1039/b407860h.

[30] Z. Li, M. Lieberman, Axial Reactivity of Soluble Silicon(IV) Phthalocyanines, Inorg. Chem. 40 (5) (2001) 932–939, https://doi.org/10.1021/ic000968w.

[31] K.M. Kane, C.R. Lorenz, D.M. Heilman, F.R. Lemke, Substituent Effects on the Spectroscopic Properties and Reactivity of Hexacoordinate Silicon(IV) Porphyrin Complexes, Inorg. Chem. 37 (4) (1998) 669–673, https://doi.org/10.1021/ic9710925.

[32] M.-E. Ragoussi, M. Ince, T. Torres, Recent Advances in Phthalocyanine-Based Sensitizers for Dye-Sensitized Solar Cells, European J. Org. Chem. 2013 (29) (2013) 6475–6489, https://doi.org/10.1002/ejoc.v2013.2910.1002/ejoc.201301009.

[33] J.Y. Zheng, K. Konishi, T. Aida, A Photoresponsive Silicon Radical within a Porphyrin π-Cloud: Photolysis of Organo- and Nitroxysilicon Porphyrins with Visible Light, J. Am. Chem. Soc. 120 (38) (1998) 9838–9843, https://doi.org/10.1021/ja980273i.

[34] H.E. Song, J.A. Cissell, T.P. Vaid, D. Holten, Photophysics of Reduced Silicon Tetraphenylporphyrin, J. Phys. Chem. B 111 (9) (2007) 2138–2142, https://doi.org/10.1021/jp0667386.

[35] J.A. Cissell, T.P. Vaid, A.L. Rheingold, An Antiaromatic Porphyrin Complex: Tetraphenylporphyrinato(Silicon)(L) 2 (L = THF or Pyridine), J. Am. Chem. Soc. 127 (35) (2005) 12212–12213, https://doi.org/10.1021/ja0544713.

[36] J. Lu, S. Liu, M. Wang, Push-Pull Zinc Porphyrins as Light-Harvesters for Efficient Dye-Sensitized Solar Cells, Front. Chem. 6 (NOV) (2018), https://doi.org/10.3389/fchem.2018.00541.

[37] M. Imran, M. Ramzan, A.K. Qureshi, M. Azhar Khan, M. Tariq, Emerging Applications of Porphyrins and Metalloporphyrins in Biomedicine and Diagnostic Magnetic Resonance Imaging, Biosensors 8 (4) (2018) 1–17, https://doi.org/10.3390/bios8040095.

[38] G.P. Moss, Nomenclature of Tetrapyrroles: Recommendations 1986, Eur. J. Biochem. 178 (2) (1988) 277–328.

[39] G.P. Moss, P.A.S. Smith, D. Tavernier, Glossary of Class Names of Organic Compounds and Reactivity Intermediates Based on Structure (IUPAC Recommendations 1995), Pure Appl. Chem. 67 (8–9) (1995) 1307–1375.

[40] D.B. Boylan, Y.I. Alturki, G. Eglinton, Application of Gas Chromatography and Mass Spectrometry to Porphyrin Microanalysis, Pergamon Press Ltd (1969), https://doi.org/10.1016/b978-0-08-006628-8.50015-0.

[41] M. Gouterman, F.P. Schwarz, P.D. Smith, D.D. Porphyrins, XXVII, Spin-Orbit Coupling and Luminescence of Group IV Complexes, J. Chem. Phys. 59 (1973) 676–690, https://doi.org/10.1063/1.1680075.

[42] J.W. Buchler, L. Puppe, K. Rohbock, H.H. Schneehage, Methoxo- Und Phenoxo-Metallkomplexe Des Octaiithylporphins Mit Zentralionen Des Typs M3@, M4e Und MO3“, Neue Wolfram- Und Rheniumporphine. *Chem. Ber.* 106 (1973) 2710–2732.

[43] J.W. Buchler, *Synthesis and Properties of Metalloporphyrins*; ACADEMIC PRESS, INC. (1978), https://doi.org/10.1016/b978-0-12-220101-1.50017-2.

[44] P.J. Marriot, J.P. Gill, G. Eglinton, Capillary Gas Chromatography and Gas Chromatography-Mass Spectrometry of Metal(III) and Metal(IV) Porphyrin Complexes, J. Chrom. 249 (1982) 291–310.

[45] P.J. Marriott, J.P. Gill, R.P. Evershed, C.S. Hein, G. Eglinton, Computerised Gas Chromatographic-Mass Spectrometric Analysis of Complex Mixtures of Alkyl Porphyrins, J. Chromatogr. 301 (1984) 107–128.

[46] J.P. Gill, R.P. Evershed, M.I. Chicarelli, G.A. Wolff, J.R. Maxwell, G. Eglinton, Computerised Capillary Gas Chromatographic Mass Spectrometric Studies of the Petroporphyrins of the Gilstonite Bitumen, J. Chromatogr. 350 (1985) 37–62, https://doi.org/10.1017/CBO9781107415324.004.

[47] C.S. Hein, J.P. Gill, R.P. Evershed, G. Eglinton, Reverse Search and Related Processing of Gas Chromatographic/Mass Spectrometric Data from Petroporphyrin Analyses, Analytical Chemistry. 57 (9) (1985) 1872–1879, https://doi.org/10.1021/ac00286a018.

[48] M. Managa, J. Britton, E. Prinsloo, T. Nyokong, Effects of Pluronic Silica Nanoparticles on the Photophysical and Photodynamic Therapy Behavior of Triphenyl-p-Phenoxy Benzoic Acid Metalloporphyrins, Journal of Coordination Chemistry. 69 (23) (2016) 3491–3506, https://doi.org/10.1080/00958972.2016.1236372.

[49] J.W. Buchler, C. Dreher, H. Gerhard, Metal Complexes with Tetrapyrrole Ligands. XLVIII. Vilsmeier Formylation of Metal Porphyrins of Cobalt(II), Nickel(II), Palladium(II), Platinum(II), Copper(II), Zinc(II), Cobalt(III), Chromium(III), Manganese(III), Iron(III), Aluminum(III), Silicon(IV), A, *Liegis Ann. Chem.* (1988) 43–54.

[50] Z. Yu, G. Sheng, J. Fu, P. Peng, Determination of porphyrin carbon isotopic composition using gas chromatography-isotope ratio monitoring mass spectrometry, J. Chromatogr. A 903 (1–2) (2000) 183–191, https://doi.org/10.1016/S0021-9673(00)00898-0.

[51] O.V. Molodkina, T.N. Lomova, E.G. Mozhzhukhina, Synthesis and reactivity of porphyrin complexes of group IV P-Elements, Russ. J. Gen. Chem. 72 (6) (2002) 968–973, https://doi.org/10.1023/A:1020407029048.

[52] T. Sugino, J. Santiago, Y. Shimizu, B. Heinrich, D. Guillon, Mesomorphic Properties of a Tetraphenylporphyrin Metallomesogen with a Weak Hydrogen Bond Interaction between Axial Ligands: Dihydroxo[5,10,15,20-Tetrakis(4-n-Dodecylphenyl)Porphinato]Silicon(IV), Liq. Cryst. 31 (1) (2004) 101–108, https://doi.org/10.1080/0267829032000159097.

[53] T. Sugino, J. Santiago, Y. Shimizu, B. Heinrich, D. Guillon, Mesomorphic properties of porphyrin silicon(IV) metal complexes, Mol. Cryst. Liq. Cryst. Sci. Technol. Sect. A Mol. Cryst. Liq. Cryst. 330 (1) (1999) 15–22, https://doi.org/10.1080/10587259908025571.

[54] S.N. Remello, F. Kuttassery, S. Mathew, A. Thomas, D. Yamamoto, Y. Nabetani, K. Sano, H. Tachibana, H. Inoue, Two-Electron Oxidation of Water to Form Hydrogen Peroxide Catalysed by Silicon-Porphyrins, Sustain. Energy Fuels 2 (9) (2018) 1966–1973, https://doi.org/10.1039/c8se00102b.

[55] S.N. Remello, F. Kuttassery, T. Hirano, Y. Nabetani, D. Yamamoto, S. Onuki, H. Tachibana, H. Inoue, Synthesis of Water-Soluble Silicon-Porphyrin: Protolytic Behaviour of Axially Coordinated Hydroxy Groups, Dalt. Trans. 44 (46) (2015) 20011–20020, https://doi.org/10.1039/c5dt03654b.

[56] J. Liu, X. Yang, L. Sun, Axial Anchoring Designed Silicon-Porphyrin Sensitizers for Efficient Dye-Sensitized Solar Cells, Chem. Commun. 49 (100) (2013) 11785–11787, https://doi.org/10.1039/c0xx00000x.

[57] B.A. Hussein, Z. Shakeel, A.T. Turley, A.N. Bismillah, K.M. Wolfstadt, J.E. Pia, M. Pilkington, P.R. Mcgonigal, M.J. Adler, Control of porphyrin planarity and aggregation by covalent capping: bissilyloxy porphyrin silanes, Inorg. Chem. 59 (18) (2020) 13533–13541.

[58] J.-Y. Zheng, K. Konishi, T. Aida, Crystallographic studies of organosilicon porphyrins: stereoelectronic effects of axial groups on the nonplanarity of the porphyrin ring, Inorg. Chem. 37 (10) (1998) 2591–2594.

[59] K.M. Kadish, Q.Y. Xu, J.M. Barbe, J.E. Anderson, E. Wang, R. Guilard, Synthesis, Photochemistry, and Electrochemistry of (P)Ge(R)2And (P)Ge(R)X (P = TPP Or OEP, R = CH3, CH2C6H5, Or C6H5, and X = C1- OH- Or C104-), J. Am. Chem. Soc. 109 (25) (1987) 7705–7714, https://doi.org/10.1021/ja00259a019.
[60] K.M. Kane, F.R. Lemke, J.L. Petersen, Trans-Difluorosilicon(IV) Complexes of Tetra-p-Tolylporphyrin and Tetrakis(p-(Trifluoromethyl)Phenyl)Porphyrin: Crystal Structures and Unprecedented Reactivity in Hexacoordinate Difluorosilanes, Inorg. Chem. 36 (7) (1997) 1354–1359, https://doi.org/10.1021/ic960639x.
[61] Z. Jian-Yu, K. Katsuaki, T. Aida, Dioxygen insertion into the axial Si-C bonds of organosilicon porphyrins, Chem. Lett. 5 (1998) 453–454.
[62] S. Ishida, T. Hatakeyama, T. Nomura, M. Matsumoto, K. Yoshimura, S. Kyushin, T. Iwamoto, A Six-Coordinate Silicon Dihydride Embedded in a Porphyrin: Enhanced Hydride-Donor Properties and the Catalyst-Free Hydrosilylation of CO2, Chem. - A Eur. J. 26 (68) (2020) 15811–15815, https://doi.org/10.1002/chem.v26.6810.1002/chem.202002587.
[63] R. Alexander, G. Eglinton, J.P. Gill, J.K. Volkman, Capillary GC and GC/MS of Bis (Trimethylsiloxy)Silicon(LV) Derivatives of Alkyl Porphyrins, Short Commun. 3 (10) (1980) 521–522.
[64] R.P. Evershed, G.A. Wolff, G.J. Shaw, G. Eglinton, Hydrogen Chemical Ionization Mass Spectrometry of Metalloporphyrins, Org. Mass Spectrom. 20 (7) (1985) 445–453, https://doi.org/10.1002/(ISSN)1096-988810.1002/oms.v20:710.1002/oms.1210200704.
[65] Z. Zhao, A.N. Cammidge, M.J. Cook, Towards Black Chromophores: μ-Oxo Linked Phthalocyanine-Porphyrin Dyads and Phthalocyanine-Subphthalocyanine Dyad and Triad Arrays, Chem. Commun. 44 (48) (2009) 7530–7532, https://doi.org/10.1039/b916649a.
[66] D.C. Lee, G.M. Morales, Y. Lee, L. Yu, Cofacial porphyrin multilayers via layer-by-layer assembly, Chem. Commun. 1 (2006) 100–102, https://doi.org/10.1039/b512084e.
[67] K. Kanaizuka, A. Izumi, M. Ishizaki, H. Kon, T. Togashi, R. Miyake, T. Ishida, R. Tamura, M.-aki. Haga, Y. Moritani, M. Sakamoto, M. Kurihara, Molecular nanostamp based on one-dimensional porphyrin polymers, ACS Appl. Mater. Interfaces 5 (15) (2013) 6879–6885, https://doi.org/10.1021/am401123r.
[68] P.C. Chambers, N.M.K. Kuruppu Arachchige, A.M. Taylor, J.C. Garno, Surface Coupling of Octaethylporphyrin with Silicon Tetrachloride, ACS Omega 4 (2) (2019) 2565–2576, https://doi.org/10.1021/acsomega.8b0320410.1021/acsomega.8b03204.s001.
[69] A. Baklanov, M. Garnica, A. Robert, M.-L. Bocquet, K. Seufert, J.T. Küchle, P.T.P. Ryan, F. Haag, R. Kakavandi, F. Allegretti, W. Auwärter, On-surface synthesis of nonmetal porphyrins, J. Am. Chem. Soc. 142 (4) (2020) 1871–1881, https://doi.org/10.1021/jacs.9b1071110.1021/jacs.9b10711.s001.
[70] T.N. Lomova, M.E. Klyueva, E.Y. Tyulyaeva, N.G. Bichan, S.V. Zaitseva, S.A. Zdanovich, A new protonated form of porphyrins in solutions, Mendeleev Commun. 22 (5) (2012) 281–283, https://doi.org/10.1016/j.mencom.2012.09.019.
[71] T.N. Lomova, M.E. Klyueva, E.G. Mozhzhukhina, E.Y. Tyulyaeva, N.G. Bichan, S. V. Zaitseva, S.A. Zdanovich, Ion-Molecular Interactions in the Metalloporphyrin-Acid System in Liquid Solutions, J. Struct. Chem. 55 (1) (2014) 180–190, https://doi.org/10.1134/S0022476614010314.
[72] J. Conradie, P.J. Brothers, A. Ghosh, Main-Group-Element Isophlorin Complexes Revisited: The Question of a Subvalent Central Atom, Inorganic Chemistry. 58 (7) (2019) 4634–4640, https://doi.org/10.1021/acs.inorgchem.9b0020110.1021/acs.inorgchem.9b00201.s001.
[73] D. Kost, I. Kalikhman, Hypervalent Silicon Compounds; Rappoport, Z., Ed.; PATAI'S Chemistry of Functional Groups, 2009. https://doi.org/10.1002/9780470682531.pat0185.
[74] A.M. Schaffer, M. Gouterman, Porphyrins - XXI. Extended Hückel Calculations on Group IV Metal Complexes, Theor. Chim. Acta 18 (1) (1970) 1–13, https://doi.org/10.1007/BF00533692.
[75] J.L. Hoard, M.J. Hamor, T.A. Hamor, J.L. Hoard, The Crystal Structure and Molecular Stereochemistry of Methoxyiron(III) Mesoporphyrin-IX Dimethyl Ester, J. Am. Chem. Soc. 87 (11) (1965) 2312–2319, https://doi.org/10.1021/ja01089a002.
[76] T. Vangberg, A. Ghosh, A first-principles quantum chemical analysis of the factors controlling ruffling deformations of porphyrins: insights from the molecular structures and potential energy surfaces of silicon, phosphorus, germanium, and arsenic porphyrins and of a peroxidase, J. Am. Chem. Soc. 121 (51) (1999) 12154–12160, https://doi.org/10.1021/ja992457i.
[77] G.J. Kang, C. Song, X.F. Ren, Effect of Meso-Submissions to Electronic Structure and Optical Properties of Ruffled Si Porphyrins Relatives, Adv. Mater. Res. 1028 (d) (2014) 7–13, https://doi.org/10.4028/www.scientific.net/AMR.1028.7.
[78] C.R. Lorenz, H.D. Dewald, F.R. Lemke, Electrochemistry of Hexacoordinate Silicon(IV) Porphyrin Complexes, Electroanalysis 9 (16) (1997) 1273–1277, https://doi.org/10.1002/(ISSN)1521-410910.1002/elan.v9:1610.1002/elan.1140091611.
[79] M. Liao, S. Scheiner, A DFT/TDDFT Study of Group 4A Metal Porphyrins, Mol. Phys. 101 (9) (2003) 1227–1238, https://doi.org/10.1080/0026897031000092931.
[80] J.P. Gill, R.P. Evershed, G. Eglinton, Comparative Computerised Gas Chromatographic-Mass Spectrometric Analysis of Petroporphyrins, J. Chromatogr. A 369 (C) (1986) 281–312, https://doi.org/10.1016/S0021-9673(00)90136-5.
[81] H. Adams, N.A. Bailey, D.W. Bruce, R. Dhillon, D.A. Dunmur, S.E. Hunt, E. Lalinde, A.A. Maggs, R. Orr, P. Styring, M.S. Wragg, P.M. Maitlis, Metallo-Mesogens and Liquid Crystals with a Heart of Gold, Polyhedron 7 (19-20) (1988) 1861–1867, https://doi.org/10.1016/S0277-5387(00)80697-X.
[82] Y. Shimizu, Photoconductivity of Discotic Liquid Crystals: A Mesogenic Long-Chain Tetraphenylporphyrin and Its Metal Complexes, Mol. Cryst. Liq. Cryst. Sci. Technol. Sect. A Mol. Cryst. Liq. Cryst. 370 (1) (2001) 83–91, https://doi.org/10.1080/10587250108030044.
[83] J. Furhop, K.M. Kadish, D.G. Davis, The Redox Behavior of Metallo Octaethylporphyrins, Pdf. *J. Am. Chem. Soc.* 16 (95) (1973) 5140–5147.
[84] K.M. Kadish, D.G. Davis, Electrochemical Studies of Metalloporphyrins, Ann. New York Acad. Sci. 206 (1) (1973) 495–503, https://doi.org/10.1149/ma2016-01/33/1623.
[85] C.R. Lorenz, H.D. Dewald, F.R. Lemke, Electrochemistry of Hexacoordinate Tetra(Aryl)Porphyrinatosilicon(IV) Complexes, Pdf. *J. Electrochem.* 415 (1996) 179–181.
[86] R. Ion, A. Sorescu, A. Nuta, New Metallo-Sensitizers in Photodynamic Therapy, Adv. Reseach Sci. Areas. (2014) 223–228.
[87] H. Ryeng, A. Ghosh, Do nonplanar distortions of porphyrins bring about strongly red-shifted electronic spectra? controversy, consensus, new developments, and relevance to chelatases, J. Am. Chem. Soc. 124 (27) (2002) 8099–8103, https://doi.org/10.1021/ja0202659.
[88] E.W. Baker, T. Fu Yen, J.P. Dickie, R.E. Rhodes, L.F. Clark, Mass Spectrometry of Porphyrins. II. Characterization of Petroporphyrins, J. Am. Chem. Soc. 89 (14) (1967) 3631–3639, https://doi.org/10.1021/ja00990a050.
[89] X. Jin, D. Li, L. Sun, C.L. Wang, F.Q. Bai, Theoretical Design of Porphyrin Sensitizers with Different Acceptors for Application in Dye-Sensitized Solar Cells, RSC Adv. 8 (35) (2018) 19804–19810, https://doi.org/10.1039/c8ra02974a.
[90] W.T. Hadmojo, D. Yim, H. Aqoma, D.Y. Ryu, T.J. Shin, H.W. Kim, E. Hwang, W. D. Jang, I.H. Jung, S.Y. Jang, Artificial Light-Harvesting n-Type Porphyrin for Panchromatic Organic Photovoltaic Devices, Chem. Sci. 8 (7) (2017) 5095–5100, https://doi.org/10.1039/c7sc01275f.
[91] H. Jensen, J.J. Kakkassery, H. Nagatani, D.J. Fermin, H.H. Girault, Photoinduced Electron Transfer at Liquid|liquid Interfaces. Part IV. Orientation and Reactivity of Zinc Tetra(4-Carboxyphenyl) Porphyrin Self-Assembled at the Water|1,2-Dichloroethane Junction, J. Am. Chem. Soc. 122 (44) (2000) 10943–10948, https://doi.org/10.1021/ja0021013.
[92] H. Xu, J.W. Aylott, R. Kopelman, T.J. Miller, M.A. Philbert, A real-time ratiometric method for the determination of molecular oxygen inside living cells using sol-gel-based spherical optical nanosensors with applications to rat C6 glioma, Anal. Chem. 73 (17) (2001) 4124–4133, https://doi.org/10.1021/ac0102718.
[93] K.P. McNamara, Z. Rosenzweig, Dye-Encapsulating Liposomes as Fluorescence-Based Oxygen Nanosensors, Anal. Chem. 70 (22) (1998) 4853–4859, https://doi.org/10.1021/ac9803232.
[94] S.H. Im, G.E. Khalil, J. Callis, B.H. Ahn, M. Gouterman, Y. Xia, Synthesis of polystyrene beads loaded with dual luminophors for self-referenced oxygen sensing, Talanta 67 (3) (2005) 492–497, https://doi.org/10.1016/j.talanta.2005.06.046.
[95] F. Kimura, G. Khalil, N. Zettsu, Y. Xia, J. Callis, M. Gouterman, L. Dalton, D. Dabiri, M. Rodriguez, Dual Luminophore Polystyrene Microspheres for Pressure-Sensitive Luminescent Imaging, Meas. Sci. Technol. 17 (6) (2006) 1254–1260, https://doi.org/10.1088/0957-0233/17/6/S04.
[96] H. Inoue, T. Okamoto, Y. Kameo, M. Sumitani, A. Fujiwara, D. Ishibashi, M. Hida, Photochemical Epoxidation of Cyclohexene Sensitized by Tetraphenylporphyrinatoantimony(V) in the Presence of Water Acting Both as an Electron and an Oxygen Donor. J. Chem. Soc. Perkin Trans. 1 1994, No. 1, 105–111. https://doi.org/10.1039/p19940000105.
[97] T. Shiragami, K. Kubomura, D. Ishibashi, H. Inoue, Efficient Photochemical Oxygenation of Cyclohexene with Water as an Oxygen Donor Sensitized by Dimethoxy-Coordinated Tetraphenylporphyrinatoantimony(V), J. Am. Chem. Soc. 118 (26) (1996) 6311–6312, https://doi.org/10.1021/ja960020u.
[98] S. Takagi, M. Suzuki, T. Shiragami, H. Inoue, Photochemical P-450 Oxygenation of Cyclohexene with Water Sensitized by Dihydroxy-Coordinated (Tetraphenylporphyrinato)Antimony(V) Hexafluorophosphate, J. Am. Chem. Soc. 119 (37) (1997) 8712–8713, https://doi.org/10.1021/ja971371r.
[99] S. Funyu, T. Isobe, S. Takagi, D.A. Tryk, H. Inoue, Highly Efficient and Selective Epoxidation of Alkenes by Photochemical Oxygenation Sensitized by a Ruthenium(II) Porphyrin with Water as Both Electron and Oxygen Donor, J. Am. Chem. Soc. 125 (19) (2003) 5734–5740, https://doi.org/10.1021/ja0295218.
[100] S. Funyu, M. Kinai, D. Masui, S. Takagi, T. Shimada, H. Tachibana, H. Inoue, Key Reaction Intermediates of the Photochemical Oxygenation of Alkene Sensitized by RuII-Porphyrin with Water by Visible Light, Photochem. Photobiol. Sci. 9 (7) (2010) 931–936, https://doi.org/10.1039/c0 pp00052c.
[101] A. Ishikawa, S. Sakaki, Theoretical study of photoinduced epoxidation of olefins catalyzed by ruthenium porphyrin, J. Phys. Chem. A 115 (18) (2011) 4774–4785, https://doi.org/10.1021/jp200650q.
[102] C. Ramesh, M. Tiwari, P. Kaur, M. Sharma, R. Jain, S. Dass, Metalloporphyrins - applications and clinical significance, Indian J. Clin. Biochem. 15 (2000) 183–199.
[103] G.Y. Tonga, K. Saha, V.M. Rotello, Interfacing nanoparticles and biology: new strategies for biomedicine, Adv. Mater. 26 (3) (2014) 359–370, https://doi.org/10.1038/jid.2014.371.
[104] S.S. Agasti, A. Chompoosor, C.C. You, P. Ghosh, C.K. Kim, V.M. Rotello, Photoregulated release of caged anticancer drugs from gold nanoparticles, J.

Am. Chem. Soc. 131 (16) (2009) 5728–5729, https://doi.org/10.1021/ja900591t.
[105] C.M. Allen, W.M. Sharman, J.E. Van Lier, Current Status of phthalocyanines in the photodynamic therapy of cancer, J. Porphyr. Phthalocyanines 5 (2) (2001) 161–169, https://doi.org/10.1002/jpp.324.
[106] K. Szaciłowski, W. Macyk, A. Drzewiecka-Matuszek, M. Brindell, G. Stochel, Bioinorganic photochemistry: frontiers and mechanisms, Chem. Rev. 105 (6) (2005) 2647–2694, https://doi.org/10.1021/cr030707e.
[107] S. Stolik, J.A. Delgado, A. Pérez, L. Anasagasti, Measurement of the Penetration Depths of Red and near Infrared Light in Human ″ex Vivo″ Tissues, J. Photochem. Photobiol. B Biol. 57 (2–3) (2000) 90–93, https://doi.org/10.1016/S1011-1344(00)00082-8.